

THE FLORIDA STATE UNIVERSITY
COLLEGE OF ARTS AND SCIENCES

VARIABILITY OF SURFACE FLUXES OVER
THE INDIAN OCEAN

By

CATHERINE STEPHENS JONES

A Thesis Submitted to the Department of
Meteorology in partial fulfillment of the
requirements for the degree of
Master of Science

Degree Awarded:

Fall Semester, 1992

Fall Semester, 1992

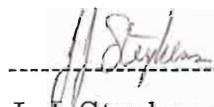
The members of the Committee approve the thesis of Catherine Stephens Jones, defended on October 29, 1992.



James J. O'Brien
Professor Directing Thesis

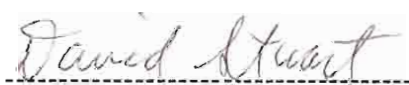


T. N. Krishnamurti
Committee Member



J. J. Stephens
Committee Member

Approved:



David Stuart, Chair, Department of Meteorology

Acknowledgments

Support for this research was provided by NASA grant NGT-30056, ONR and NOAA.

I would like to express my appreciation to my advisor, Dr. James O'Brien, for his guidance and encouragement. He was instrumental in all aspects of my graduate career at Florida State. I would also like to thank him for the opportunities with which he provided me as an undergraduate and graduate student.

In addition, I would like to thank the members of my committee, Dr. Stephens and Dr. Krishnamurti, for their input in this research. I also appreciate their contribution to my overall education.

Special gratitude goes to Dr. David Legler whose assistance was essential to the completion of this project. Thanks also to my fellow MASIGists who helped prepare the final plots, movies and etc.

Finally, I am especially grateful to my husband, Bill, who gave me constant encouragement and support throughout graduate school, even from long distance.

Table of Contents

	Page
Acknowledgments	iii
List of Figures	v
List of Tables.....	vii
Abstract	viii
1. INTRODUCTION.....	1
2. DATA SET.....	9
2.1 COADS data set.....	9
2.2 Flux calculations.....	10
2.3 Climatologies of surface parameters.....	12
3. OBJECTIVE ANALYSIS TECHNIQUE.....	23
3.2 Weight selection.....	26
4. RESULTS.....	32
4.1 Mean maps.....	32
4.2 Variability of surface fluxes.....	41
4.3 EOF analysis.....	47
5. SENSITIVITY ANALYSIS.....	53
6. CONCLUSIONS AND SUMMARY.....	58
7. APPENDIX: Monthly mean results.....	61
References.....	70
Biographical Sketch.....	74
Biographical Sketch.....	74

List of Figures

	Page
Figure 1. The Florida State University tropical Indian Ocean winds demonstrate (a) the wind flow pattern of the winter monsoon in January and (b) the reversal of winds during the summer monsoon in July.....	3
Figure 2. Climatologies of the surface parameters obtained from the COADS data set for the period 1960-1989 are shown. The months of January, April, July and October are considered representative of each season. These months are shown for the SST (a-d); the AT (e-h); the Q (i-l); and the W (m-p).....	15
Figure 3. The input and resultant fields of the surface variables using the optimal weights for the August 1965 case: (a-b) SST; (c-d) AT; (e-f) Q; (g-h) W; and (i-j) psuedo-stress vectors.....	34
Figure 4. The resultant fields, using the optimal weights, of (a) latent heat flux, (b) sensible heat flux, and (c) wind stress for August 1965.....	39
Figure 5. The difference in the average wind speed of the sixties and the eighties is shown.....	44
Figure 6. The difference in the average latent heat flux in the sixties and the eighties is shown.....	45

Figure 7. (a) Time series of the first eigenvector of latent heat flux with a 12-month moving average. (b) The spatial pattern of the first eigenmode of latent heat flux.....47

Figure 8. (a) The time series of the first eigenvector of the wind stress corresponding to 73% of the variance. The 12-month moving average is superimposed (thicker line) to indicate the trend. (b) The spatial structure of the first eigenmode of wind stress.....52

Figure 9. The local sensitivity of (a) latent heat flux and (b) wind stress due to the relative uncertainty of the optimal weights.....57

Figure 10. Monthly mean resultant fields for January 1976 are shown: (a) SST; (b) AT; (c) Q; (d) W; (e) latent heat flux; (f) sensible heat flux; (g) pseudo-stress vectors and (h) wind stress vectors.....62

Figure 11. Monthly mean resultant fields for July 1984 are shown: (a) SST; (b) AT; (c) Q; (d) W; (e) latent heat flux; (f) sensible heat flux; (g) pseudo-stress vectors and (h) wind stress vectors.....66

List of Tables

	Page
Table 1. Quantitative error analysis.....	28
Table 2. Optimal weights.....	31
Table 3. Relative sensitivities of the optimal weights	56

Abstract

A variational-direct minimization objective analysis technique is used to create a set of regularly spaced monthly mean maps from 1960-1989 of temperature, wind, humidity, sensible and latent heat flux and wind stress over the Indian Ocean using the Comprehensive Ocean-Atmosphere Data Set as input. The technique simultaneously solves for all the fields listed above through a coupled relationship between the flux parameterizations and the solution fields. The variational method utilizes a set of constraints which express a lack of fit to input data, climatology and kinematics.

The variation of latent heat flux in the Indian Ocean contains a large annual component and is related to the strength of the monsoon winds. The sea surface temperature exerts a secondary influence on the latent heat flux. On a monthly time scale, latent heat flux is always from the ocean to the atmosphere. Maximum values of latent heat flux are found in trade winds and the Arabian Sea during the southwest monsoon. Minimum values of latent heat flux are observed during the northeast monsoon over the entire domain. Sensible heat flux is less variable than latent heat flux and is more dependent on the air-sea temperature difference.

An Empirical Orthogonal Function (EOF) analysis of latent heat flux indicates: (1) large decadal variability with a biannual signal during the seventies; (2) a strong correlation with Indian rainfall; and (3) no correlation to El Niño.

1. INTRODUCTION

Surface fluxes of heat and momentum provide the link in the interaction between the atmosphere and ocean. This relationship is vital to the understanding of weather and climate in the tropics. However, the formulae used to estimate the surface fluxes are a function of several meteorological and oceanographical variables which may not be adequately measured. Many scientists have estimated climatologies of surface fluxes for the global oceans as well as for specific regions. Hastenrath and Lamb (1979) published an atlas of the oceanic heat budget in the Indian Ocean. Similarly, Oberhuber (1988) and Congbin *et al.* (1990) created atlases of the net heat budget and surface heat fluxes, respectively, over the global oceans. Meanwhile, Hsiung (1986) studied the annual and monthly means of the surface energy fluxes over the global oceans. Weare *et al.* (1981) studied the long term annual mean of net surface heating in the tropical Pacific.

All of the above studies were focused on the climatological and/or mean annual estimates of the surface fluxes. The research contained in this paper creates a consistent set of monthly maps of surface fluxes and surface parameters in the Indian Ocean basin for a 30-year period (January 1960 - December 1989). The data set is obtained from the Comprehensive Ocean Atmosphere Data Set (COADS). Missing data due to the absence of ship reports or erroneous measurements are replaced by an
Comprehensive Ocean Atmosphere Data Set (COADS). Missing data due to the absence of ship reports or erroneous measurements are replaced by an

objective analysis technique developed previously by Legler (1992) over the North Atlantic Ocean.

A consistent set of monthly fields of the surface fluxes does not exist. Data are particularly sparse over the Indian Ocean. Previous studies have examined single variables (*i.e.* sea surface temperature, wind speed, *etc.*) and their relationships to the monsoon. This is the first study which jointly solves for and examines the surface fluxes and the surface variables which determine the fluxes. Better estimates of the surface fluxes and an estimate of their uncertainty will permit a determination of the importance of the fluxes in the atmosphere and upper ocean thermodynamics.

The monsoon systems of India, northeast Africa, southeast Asia and the continent of Australia are driven by this air-sea interaction. The southeast trade wind belt west of Australia, the Bay of Bengal and the Arabian Sea are of particular interest in the Indian Ocean regime. In addition, improved surface flux analyses may clarify the spatial and temporal variability influenced by such large scale phenomena as the El Niño Southern Oscillation (ENSO) and the Indian summer monsoon.

The most predominant phenomenon found in the Indian Ocean is the annual monsoon reversal. The physical parameters of the atmosphere and ocean as well as the flux or transport quantities demonstrate considerable variability in relation to the summer and winter monsoons. In general, the summer monsoon in the lower atmosphere is dominated by strong westerly and southwesterly flow across south and central India (Figure 1). Strong southeasterly trade winds are found in the Southern strong westerly and southwesterly flow across south and central India (Figure 1). Strong southeasterly trade winds are found in the Southern

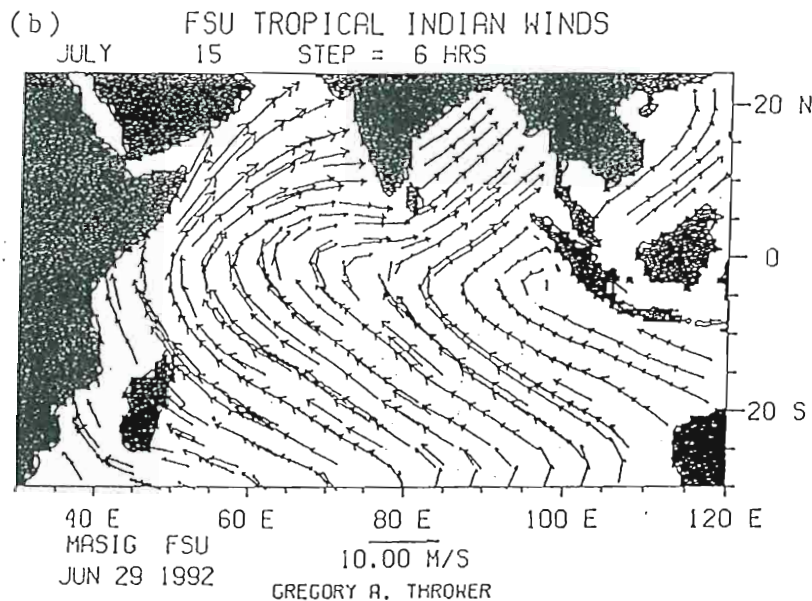
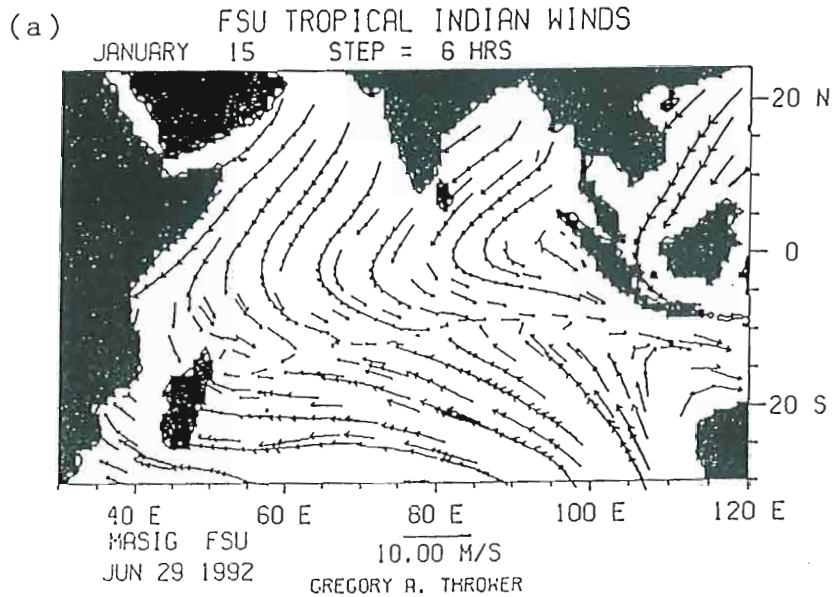


Figure 1. The Florida State University tropical Indian Ocean winds demonstrate: (a) the wind flow pattern of the winter monsoon in January. Strong northeasterlies are observed in the northern Indian Ocean. (b) The reversal of winds is observed in the summer monsoon flow during July. Strong southwesterlies off the coast of Somalia flow into the Arabian Sea and Bay of Bengal, bringing a lot of moisture into India.

Hemisphere. Likewise, strong cross-equatorial flow is observed along the east coast of Africa in association with the low-level Somali jet. The cross-equatorial flow acquires moisture over the southern Indian Ocean, transports the moisture into the Arabian Sea and brings rain to India. The air is nearly saturated (Cadet and Diehl, 1984).

The winter monsoon is dominated by a reversal of flow. Northeasterlies prevail over the China Sea, Bay of Bengal and Arabian Sea. The northern and southern trades converge at 10-20°S as the Indian Ocean resembles the Atlantic and Pacific Oceans with two tradewind systems present (Knox, 1986). More information is available on the summer monsoon as the intensity is much stronger.

Although the monsoons are predominately characterized by their overall flow patterns, the intensity of the monsoon is correlated to other surface parameters. Shukla and Misra (1977) considered the importance of air-sea interaction to the intensity of the monsoon circulation and precipitation. They stated that higher wind speeds over the Arabian sea were correlated with lower sea surface temperatures. The stronger winds led to an increase in evaporation as well as to an increase in upwelling and spreading of cold coastal waters.

The negative correlation was also noted by Cadet and Diehl (1984) who examined the interannual variability of the sea surface temperature, air temperature, surface pressure, surface wind and the mixing ratio in relation to the intensity of the monsoon. They determined that weaker than normal trade winds in the Southern Hemisphere and stronger zonal winds relation to the intensity of the monsoon. They determined that weaker than normal trade winds in the Southern Hemisphere and stronger zonal winds along the eastern coast of Africa were associated with a deficit of rainfall

over India during the summer. In addition, warmer sea surface temperature over the Indian Ocean in the summer was responsible for weak atmospheric circulation found during a dry monsoon period. Conversely, colder sea surface temperature was responsible for stronger atmospheric forcing during a wet monsoon.

This link between sea surface temperature and rainfall is weak according to Weare (1979). Although warmer sea surface temperatures led to a stronger monsoon, higher sea level pressures tend to offset the effects of temperature on rainfall.

More recently, interest in the correlation between the Indian summer monsoon and ENSO has developed. Again, a negative correlation between the Indian Ocean sea surface temperature and the monsoon is indicated. Weare (1989) suggested that the weakened latent heat fluxes in the eastern Pacific acted to reinforce the warming of the ocean surface in the early stages of El Niño. Philander and Hurlin (1988) suggested that a developed El Niño increased the latent heat flux which occurred during the warm water phase of ENSO. Furthermore, Verma (1992) established correlation maps between the monsoon precipitation from June to September and sea surface temperature anomalies in the Pacific from March to December. Verma suggested the warmer phase of ENSO was associated with weaker monsoon activity, or less precipitation. The cooler phase of ENSO was associated with a stronger monsoon and more precipitation. However, the signal was not considered strong enough to forecast the Indian monsoon precipitation.

precipitation. However, the signal was not considered strong enough to forecast the Indian monsoon precipitation.

Since latent heat flux and sensible heat flux are related to sea surface temperature, wind and humidity, their importance to the monsoon is naturally assumed. Latent heat release is the primary component of ocean to atmosphere heat exchange (Congbin *et al.*, 1990). Maximum values are observed along the eastern coasts of continents due to the boundary contrasts between the continents and the downwind ocean. Minimum values are found in upwelling regions such as the Arabian peninsula during the summer monsoon and the South China Sea during the winter monsoon. On a monthly time scale, the transport of latent heat is almost always from the ocean to the atmosphere. On the other hand, sensible heat is transported from the atmosphere to the ocean (negative values) off the eastern coasts of continents when upwelling occurs.

Annual values and patterns of latent and sensible heat flux are related to the Northern Hemisphere summer monsoon. Hastenrath and Lamb (1980) studied the ocean heat budget of surface heat fluxes determined from long term ship observations and satellite data. During the northern summer, sensible and latent heat are released by the ocean. Moisture is evaporated from the southern tropical Indian Ocean and carried across the equator in the monsoonal flow. The moisture is then released as precipitation over southern Asia.

Knox (1986) notes a surface exchange of heat from the atmosphere to the ocean in the Arabian Sea during the summer despite the strong winds. However, this exchange is offset by the heat flux across the equator due to the northerly flow of cooler water from the Somali current. Upwelling along
However, this exchange is offset by the heat flux across the equator due to the northerly flow of cooler water from the Somali current. Upwelling along

the African and Arabian coasts leads to the cooling of the ocean in the northern summer and warming in the winter.

Latent and sensible heat fluxes have major impacts on the large scale sea surface temperature anomaly field in the mid-latitudes (Cayan, 1990). Only a few studies have tested the relationship between the fluxes and the sea surface temperature field over broad scales. These include an observational study (Frankignoul and Reynolds, 1983) and an ocean general circulation model (Haney, 1985). Both studies indicated that anomalous heating by the surface fluxes were a major component in producing monthly thermal anomalies in the North Pacific Ocean.

By examining the surface fluxes in relation to six surface parameters, sea surface temperature, air temperature, specific humidity, the scalar wind and pseudo-stress wind components of the COADS data, it is found that higher latent heat flux is associated with stronger winds. In the central Arabian Sea, latent heat flux is related also to the sea surface temperatures along the coasts of Somalia and the Arabian peninsula. Regions of strong coastal upwelling reduce the latent heat flux.

A negative correlation exists between the western coast of Australia and the Arabian Sea. Higher latent heat flux in the trade winds off the western coast of Australia is observed during the drier Indian monsoon periods. During these years, the equatorial trough deepens over the Australian continent and more moisture is present during the summer Australian monsoon.

In the following pages, section 2 describes the data sets and the bulk Australian monsoon.

In the following pages, section 2 describes the data sets and the bulk formulae used in computing the surface fluxes. The objective analysis

technique and the connectivity of the terms are described in section 3. Results of the objective analysis and the variability of the results are discussed in section 4. EOF analyses indicate large annual and decadal variability in latent heat flux. Meanwhile, the wind stress only contains large annual variability. Although a strong correlation is established between latent heat flux and Indian rainfall, no correlation between the latent heat flux and El Niño is found. Section 5 discusses the sensitivity of the scheme. Wind stress and latent heat flux solutions are more sensitive to the optimal weights of the sea surface temperature wind speed terms than the other weights. Finally, the conclusions and findings are recapped in section 6.

2. DATA SET

2.1 COADS data set

The COADS data are monthly means of individual meteorological reports from ships of opportunity, meteorological buoys and ocean weather ships. The data are stored in quality controlled reports and summaries on a 2° latitude by 2° longitude grid. Data which fell outside 2.8 standard deviations of the median of each of the 2° by 2° boxes were trimmed from this data set. Likewise, duplicate data records were also removed from the COADS data set (Slutz *et al.*, 1985).

Monthly means of sea surface temperatures (SST), air temperatures (AT), specific humidity (Q), scalar wind speed (W) and pseudo-stress wind components (the product of the directional wind component and the scalar wind, UW and VW) over the Indian Ocean region (30°S to 24°N , 30°E to 120°E) are extracted from COADS during the period 1960 to 1989. The pseudo-stress components of wind are henceforth noted simply as the wind components. This grid yields 888 stations over the ocean. Approximately 95% of the stations record measurements for any given month. Thus, data distribution is dense.

2.2 Flux calculations

The bulk formulae are a practical means of estimating air-sea exchanges and many uses are noted. Since the distribution of COADS data is highly variable in space and time, some caution is advised. However, Cayan (1990) considers one month a convenient time scale in which to examine fluxes. He notes that one month is long enough to average over several events for more statistical significance, but also short enough to retain the details of magnitude and structure in the heat transfers over the ocean. Esbensen and Reynolds (1981) observe that surface heat fluxes calculated using monthly means did not differ greatly from the monthly averaged heat fluxes calculated from daily data.

For monthly means, the largest variations in space and time of the heat fluxes generally arise from the variations in space and time of W and Q . The latent heat flux is also more affected by the horizontal temperature gradient than is the sensible heat flux. Higher values of latent heat flux are observed at low latitudes because of the larger values of Q , SST and AT . Therefore, areas dominated by the trade winds and western boundary currents produce a maximum of latent heat transfer. Sensible heat is comparatively small due to the weak temperature gradient. Several exceptions to this occur when cold air masses of continental origin flow over warm water at high speeds as are observed in the Gulf Stream and the Kuroshio.

As direct measurements of surface fluxes are rarely available, the Kuroshio.

As direct measurements of surface fluxes are rarely available, the bulk aerodynamic formulae are used to calculate these surface fluxes of

momentum and sensible and latent heat. Several methods of calculating surface fluxes have been previously attempted. Large and Pond (1982) used the eddy correlation and dissipation methods. However, they found little difference between the time variations of fluxes for the bulk formulae versus those determined by the eddy correlation and dissipation methods for time averages. Thus, the bulk formulae are used in this paper and are defined as:

$$H = \rho_a c_p W (SST - AT)$$

$$E = \rho_a c_r W (Q_{ssfc} - Q)L$$

$$\tau_x = \rho_a c_d UW$$

$$\tau_y = \rho_a c_d VW$$

where ρ_a is the density of air, c_p is the specific heat at constant pressure ($1004 \text{ J kg}^{-1} \text{ C}^{-1}$), L is the latent heat of vaporization ($2.5 \times 10^6 \text{ J kg}^{-1}$) and c_0 , c_r and c_d are the drag coefficients. The Q_{ssfc} term denotes the sea surface specific humidity and is calculated from the sea surface temperature, surface pressure and the dewpoint temperature. The Q and AT are considered to be measured at 10 meters typically on a ship; the winds are assumed to be measured at 20 meters. The rate of energy exchange (sensible heat, H , and latent heat, E) is expressed in W m^{-2} , stress (τ) in N m^{-2} . Positive heat flux values indicate a gain of thermal energy by the atmosphere. For wind stress calculations, using pseudo-stress components rather than actual wind components is critical; it reduces the difference

between the stress from the means of coincident stress and the stress calculated using the mean winds (Hanawa and Toba, 1987).

The largest uncertainty in the fluxes depends on how the bulk formulae are applied. For this study, the bulk coefficients c_θ , c_r and c_d of Smith (1988) are used. The coefficients c_d and c_θ depend strongly on the air-sea virtual potential temperature difference at low wind speeds. However, higher wind speeds decrease the dependency of the coefficients on the temperature difference.

2.3 Climatologies of surface parameters

Climatologies of the surface variables (SST, AT, Q and W), extracted from the COADS data set, were created. The climatological fields primarily reflect the summer and winter monsoonal weather patterns and are consistent with those of Hastenrath and Lamb (1979) and Wright (1988). For pseudo-stress components, the Florida State University climatologies developed from Legler, *et al.* (1989) are used.

The largest values of the SST are generally found in the northern region of the Indian Ocean and the overall orientation is zonal (Figure 2a-d). The summer months show the highest values of SST to be north of the equator in the South China Sea, the Arabian Sea and the Bay of Bengal with values at 29°C. South of 20°S, cooler temperatures ranging between 19°C and 22° are recorded. As the monsoon reaches its peak in August, a slight temperature gradient is observed off the Arabian peninsula due to the and 22° are recorded. As the monsoon reaches its peak in August, a slight temperature gradient is observed off the Arabian peninsula due to the strong winds and upwelling. Maximum SST values in the winter are

located near the equator. A large gradient is observed in the South China Sea where the northeastern trades are strong. Some upwelling is also occurring off the China coast in association with the winter monsoon.

The AT climatology (Figure 2e-h) is similar to the SST. Over the North Indian Ocean, the atmosphere and ocean temperatures vary less than 1° Celsius throughout the year. South of the equator, the atmosphere is 2-3° cooler than the ocean. The winter air temperature picture indicates the same gradient as the SST off the China coast with the largest temperatures centered near the equator. During the summer, the air temperature demonstrates a sharper decline south of 10°S.

The specific humidity is generally higher north of 10°S regardless of the season (Figure 2 i-l). During the summer months, Q increases north of the equator as the winds transport more moisture into the North Indian Ocean. Values are 21 g kg⁻¹ as opposed to 18 g kg⁻¹ in the northern winter. However, in the late fall, the highest values of Q are found in the Bay of Bengal and in the southern hemisphere tropics. Both areas are under the influence of the winter monsoon at this time.

The scalar wind speed (Figure 2 m-p) and pseudo-stress wind vector climatologies demonstrate the onset of the summer and winter monsoons, as well. During the summer, winds are strongest off the Arabian coast and are on the order of 10 - 14 m s⁻¹. Moderately strong winds exist in the Bay of Bengal and in the latitudinal band 10 - 20°S. The southeasterly trade winds increase as the summer monsoon develops. Likewise, the Somali jet increases and strengthens the westerly and westsouthwesterlies over the increase as the summer monsoon develops. Likewise, the Somali jet increases and strengthens the westerly and westsouthwesterlies over the Arabian Sea. The overall flow pattern in the winter is the reverse of the flow

during the summer monsoon for the Indian Ocean region. The strongest winds occur off the eastern coast of Asia over the South China Sea in the northern winter. These are the northeast trade winds which are indicative of the flow pattern. Northeasterlies also dominate the Arabian Sea and flow southward down the east African coast. The spring and fall wind patterns are very weak over the entire basin.

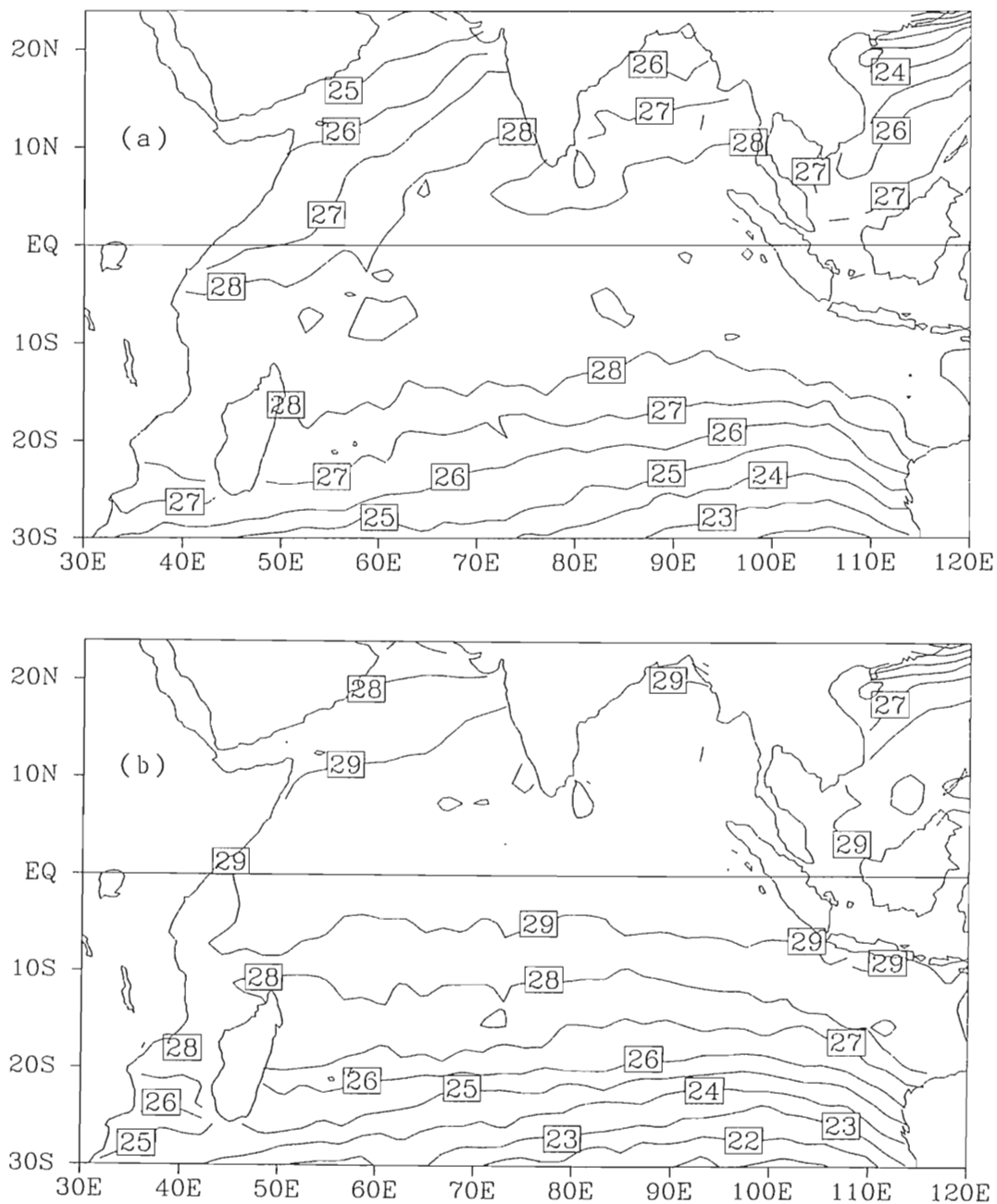


Figure 2. Climatologies of the surface parameters obtained from the COADS data for the period 1960-1989 are shown. The months of January, April, July and October are considered representative of each season. These months are shown for the SST (a-d); the AT (e-h); the Q (i-l); and the W (m-p). Contour intervals for the SST and AT are 1°C . The contour intervals for Q are 1 g kg^{-1} and 1 m s^{-1} for W.

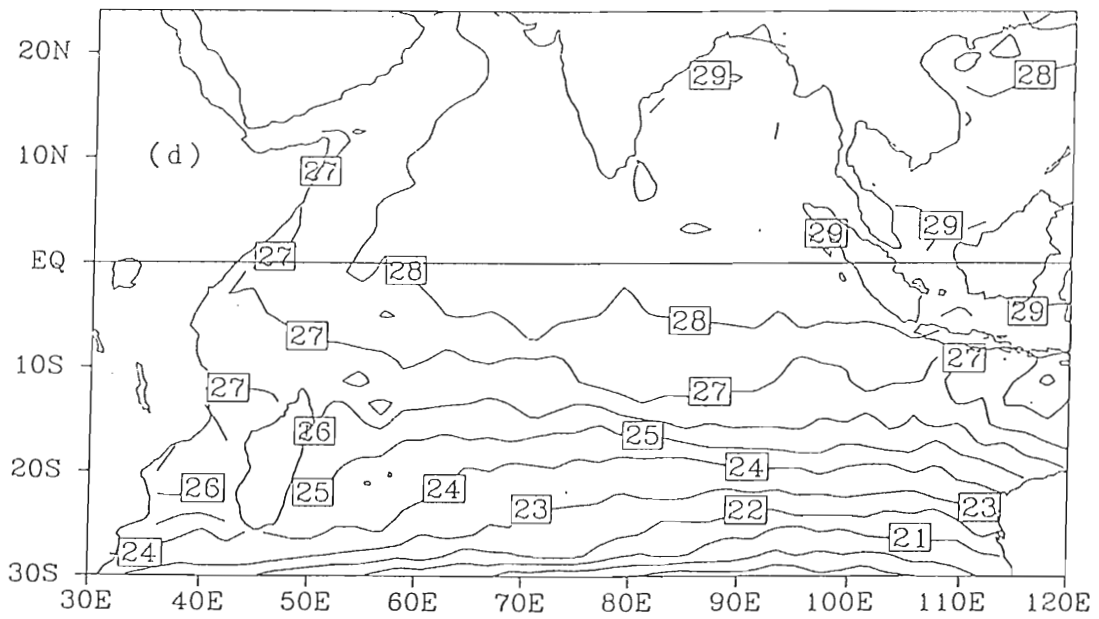
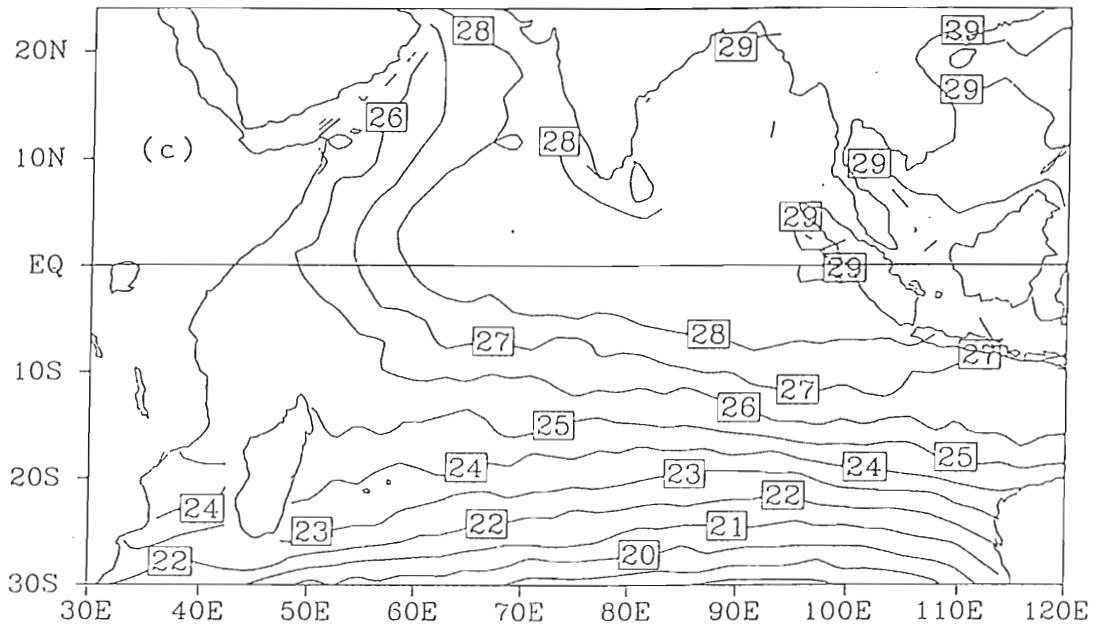


Figure 2. (Continued)

Figure 2. (Continued)

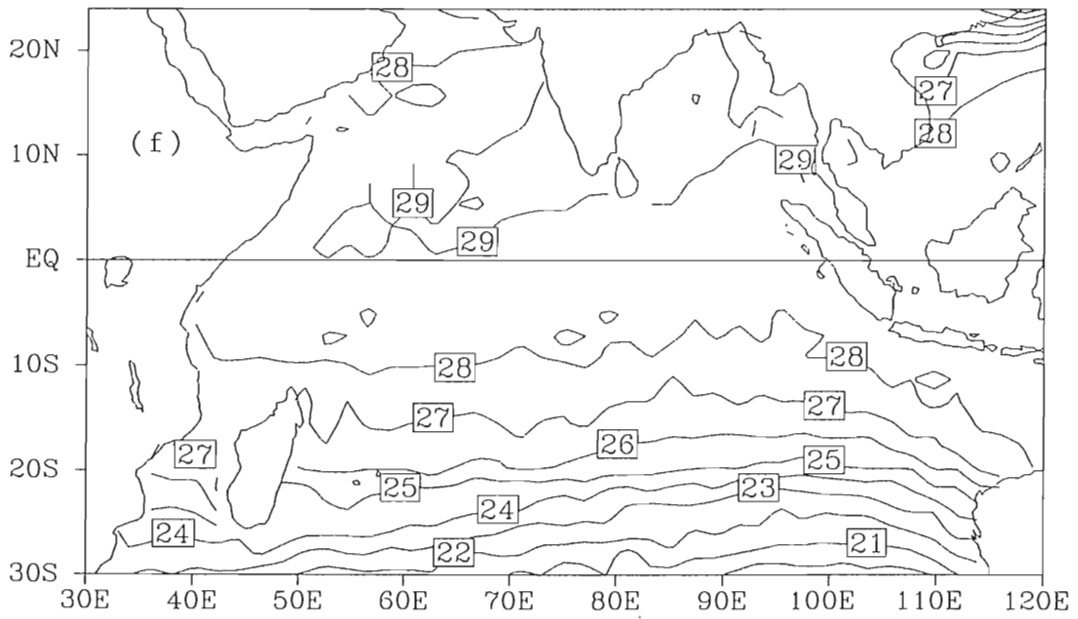
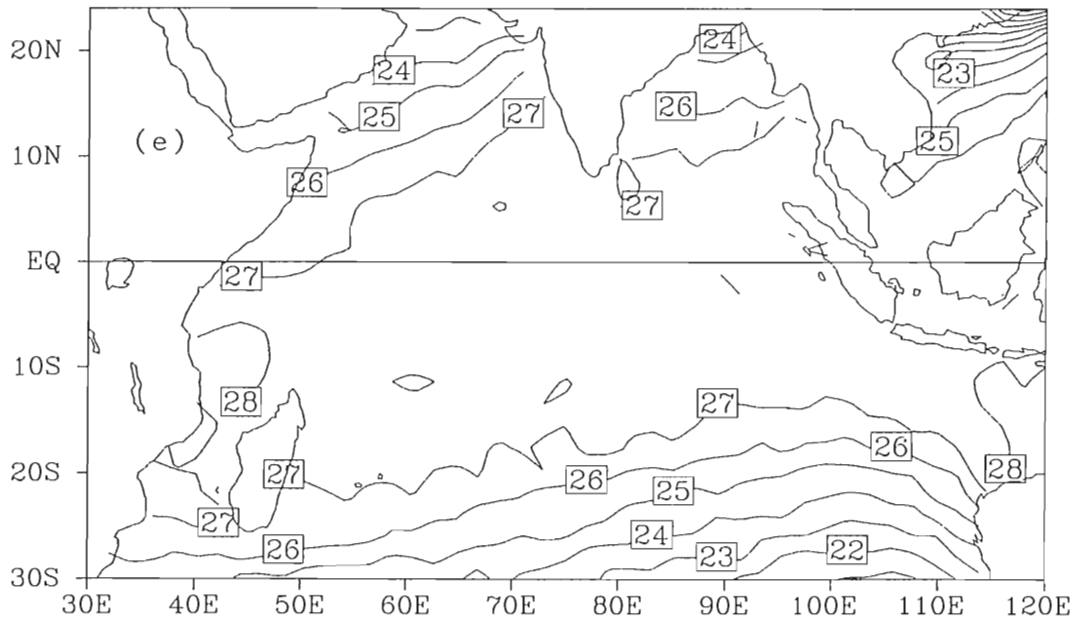


Figure 2. (Continued)

Figure 2. (Continued)

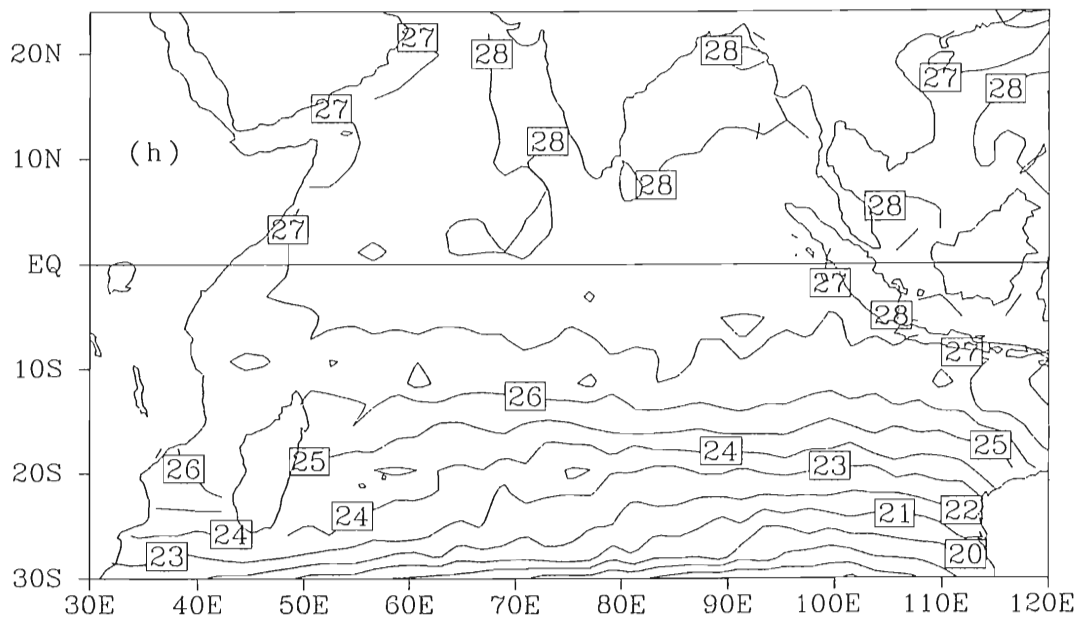
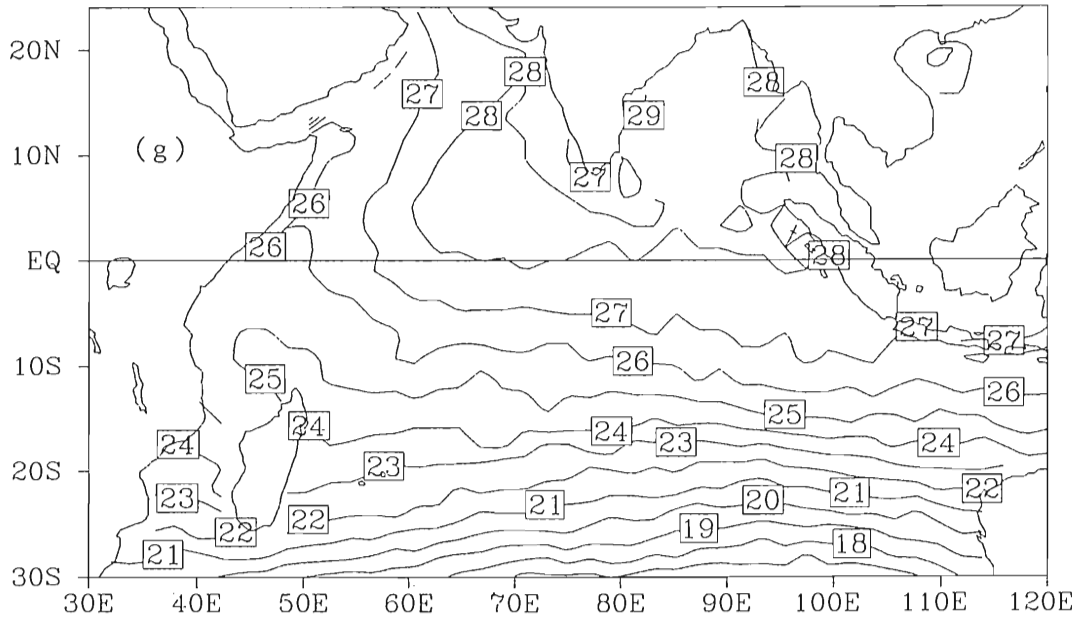


Figure 2. (Continued)

Figure 2. (Continued)

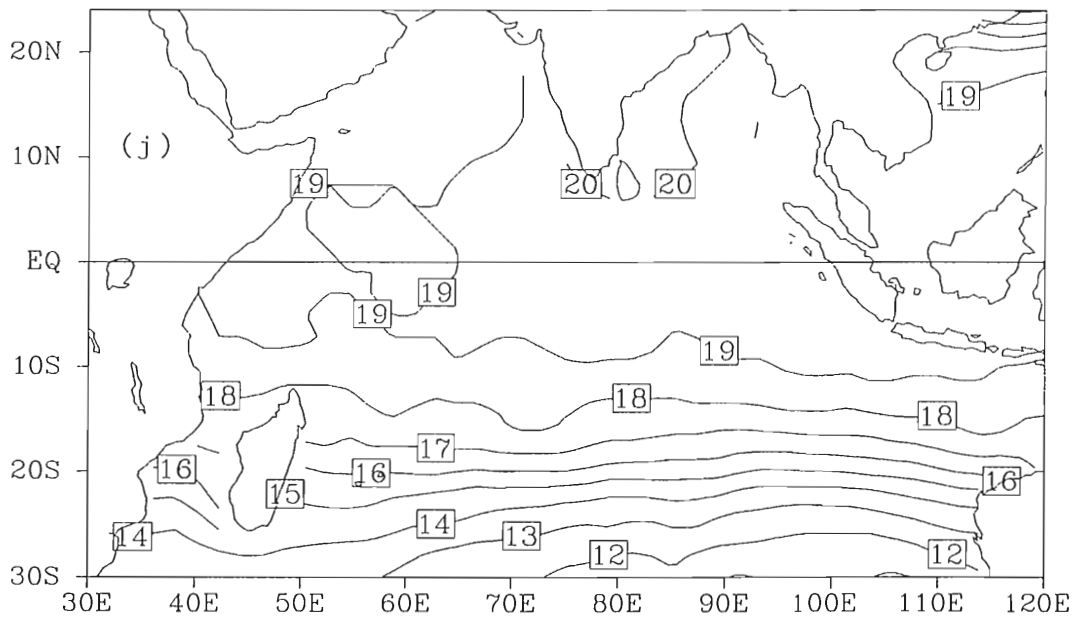
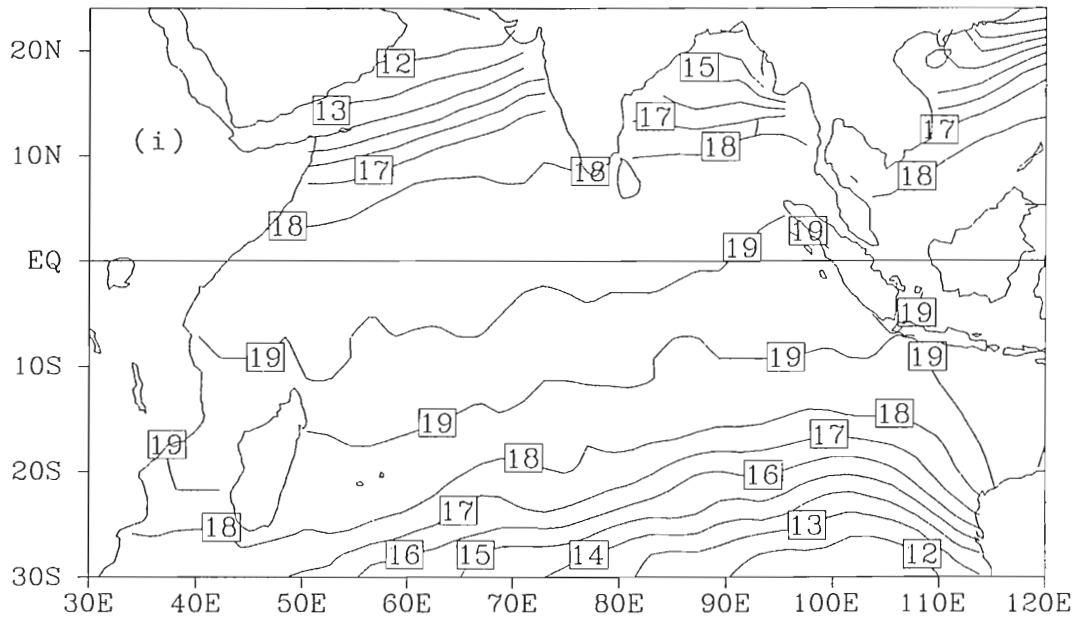


Figure 2. (Continued)

Figure 2. (Continued)

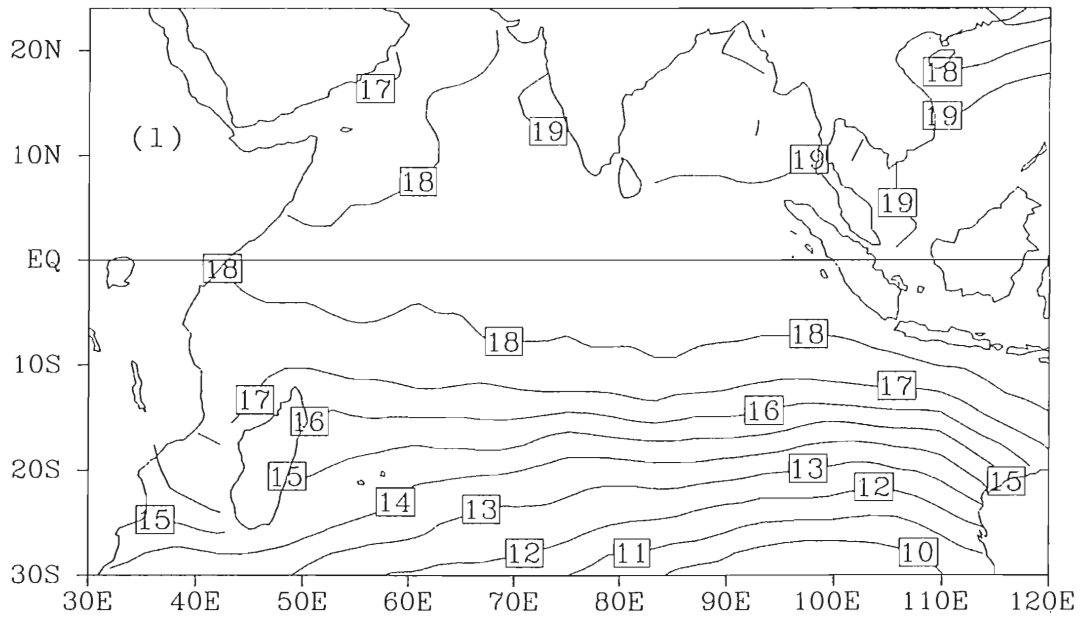
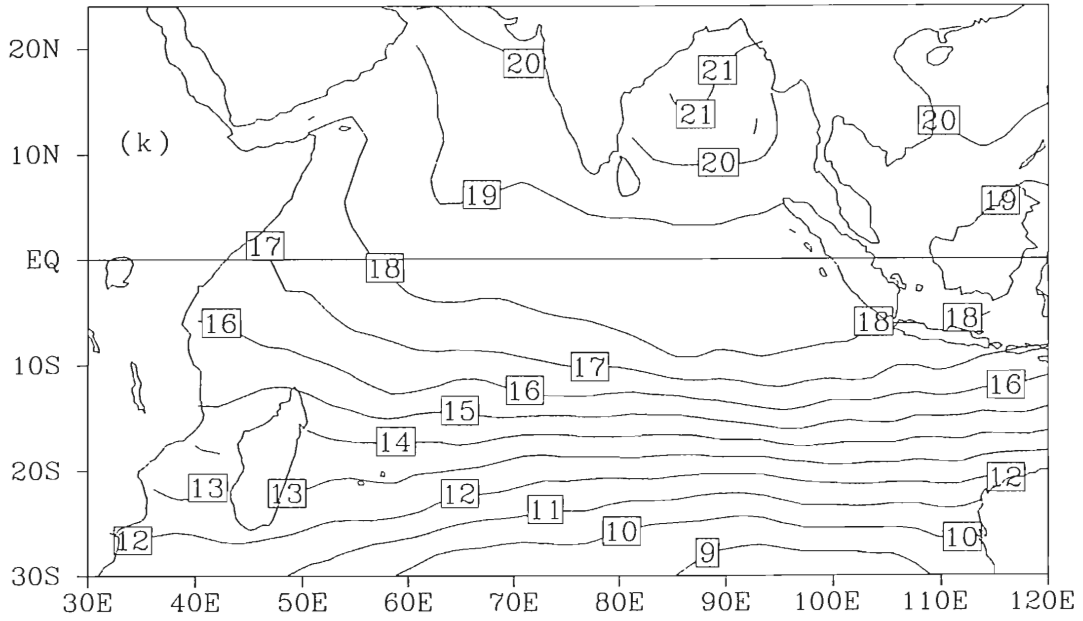


Figure 2. (Continued)

Figure 2. (Continued)

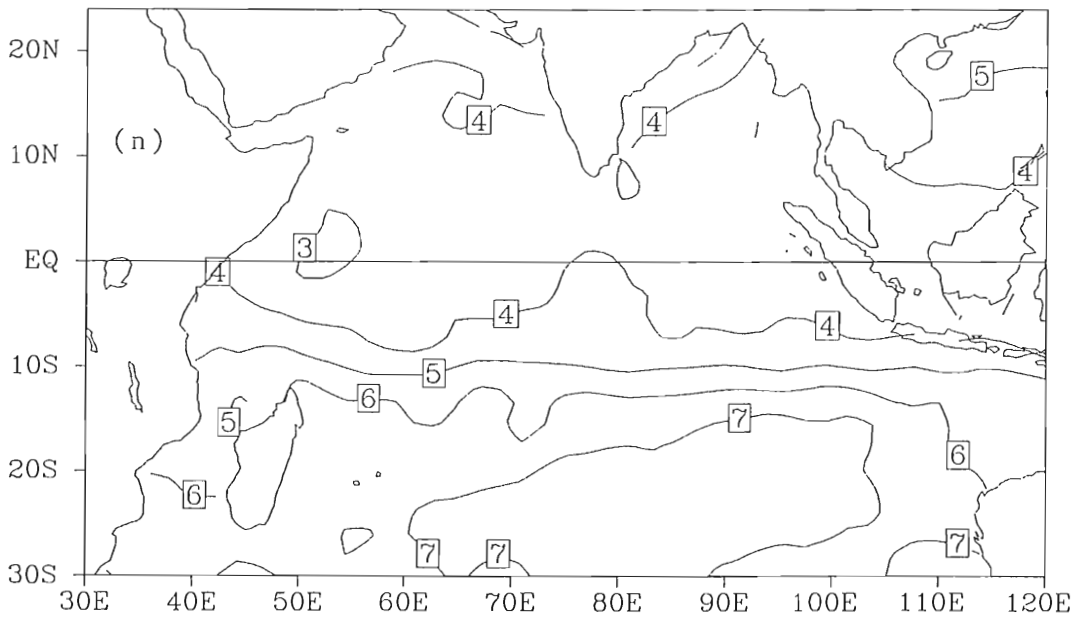
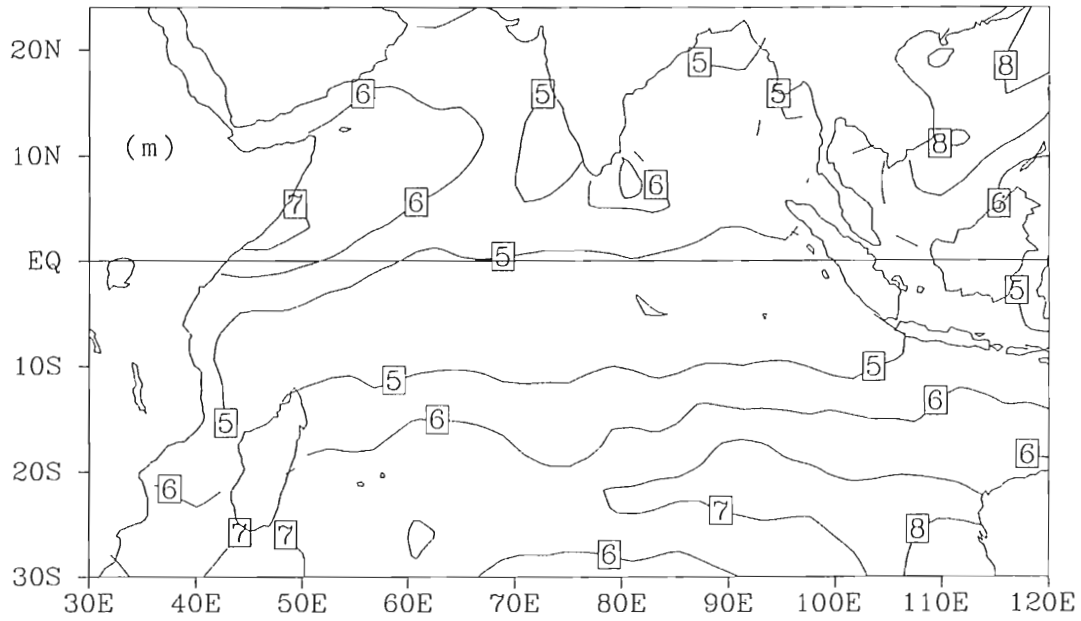


Figure 2. (Continued)

Figure 2. (Continued)

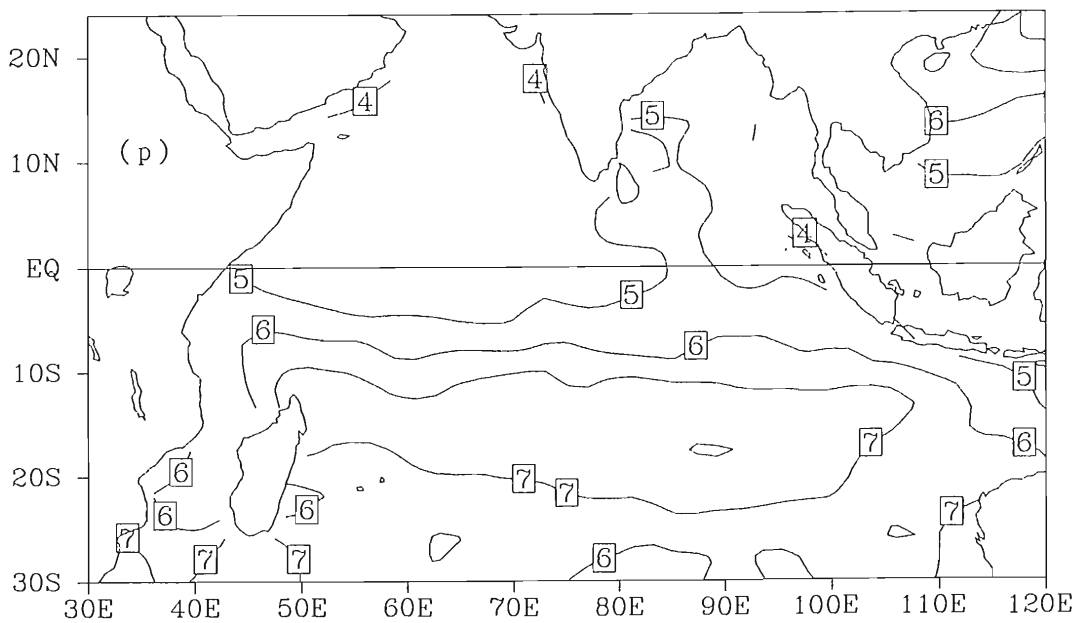
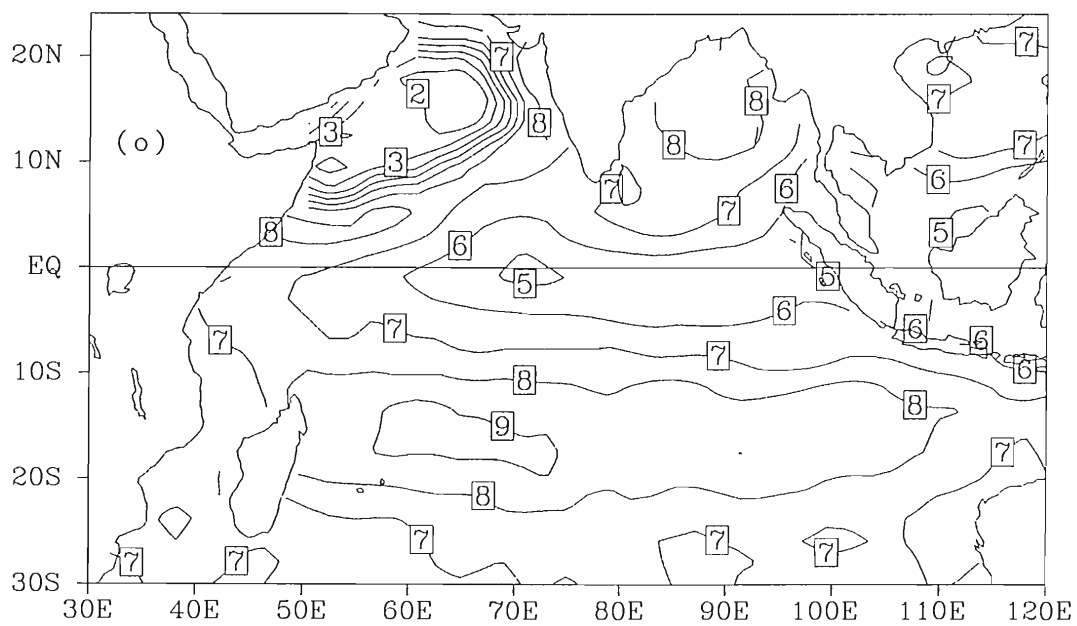


Figure 2. (Continued)

Figure 2. (Continued)

3. OBJECTIVE ANALYSIS METHOD

Variational analysis methods allow information in various forms to be combined by minimizing a lack of fit to a set of constraints. This technique was documented by Sasaki (1955) and previously employed by Legler (1992) to determine surface fields over the Atlantic Ocean, by Hoffman (1984) in order to remove the ambiguity of SeaSat satellite scatterometer winds (SASS), and by Legler *et al.* (1989) to formulate surface pseudo-stress vectors in the Indian Ocean. The functional used must retain information from the input ship data, some information of the climatic norm and information on the covariant structure. The random errors in the input ship data are assumed to be normally distributed. The method is similar to a constrained least squares method which involves direct minimization of a cost functional consisting of 17 terms and which is implemented over the Indian Ocean basin. Each term represents a measure of lack of fit to certain conditions driven by dynamics and/or statistics. Associated with each term is an empirically determined weight.

The cost functional in this study is used to create objectively analyzed monthly maps of the surface variables such as temperature, humidity and winds. In addition, monthly fields of the derived fluxes, latent and sensible heat and wind stress, are created. The first six terms of this functional describe expressions of misfit to the input data from COADS; the next four heat and wind stress, are created. The first six terms of this functional describe expressions of misfit to the input data from COADS; the next four terms are constraints which force the resultant fluxes to approximate the

COADS flux fields; the next six terms smooth the results by forcing the resultant fields to resemble climatology in a smooth sense; and the final term is a kinematic constraint which approximates the expected curl of the pseudo-stress wind field. The functional is:

$$\begin{aligned}
 F = & \alpha \sum (SST - SST_{coads})^2 + \beta \sum (AT - AT_{coads})^2 \\
 & + \gamma \sum (Q - Q_{coads})^2 + \delta \sum (W - W_{coads})^2 \\
 & + \epsilon \sum (WU - WU_{coads})^2 + \phi \sum (WV - WV_{coads})^2 \\
 & + \Gamma \sum (H_S - H_{coads})^2 + \eta \sum (E_V - E_{coads})^2 \\
 & + \xi \sum (\tau_x - \tau_{xcoads})^2 + \zeta \sum (\tau_y - \tau_{ycoads})^2 \\
 & + \rho L^4 \sum (\nabla^2(SST - SST_{cl}))^2 + \Lambda L^4 \sum (\nabla^2(AT - AT_{cl}))^2 \\
 & + \mu L^4 \sum (\nabla^2(Q - Q_{cl}))^2 + \nu L^4 \sum (\nabla^2(W - W_{cl}))^2 \\
 & + \sigma L^4 \sum (\nabla^2(UW - UW_{cl}))^2 + \Pi L^4 \sum (\nabla^2(VW - VW_{cl}))^2 \\
 & + \Theta L^2 \sum (\hat{k} \cdot \nabla \times (\vec{V}W - \vec{V}W_{cl}))^2
 \end{aligned}$$

The symbols in the functional are as follows:

SST_{coads}	COADS Sea Surface Temperature
AT_{coads}	COADS Air Temperature
Q_{coads}	COADS Specific Humidity
W_{coads}	COADS Wind Speed
UW_{coads} and VW_{coads}	COADS Pseudo-Stress components
E_{Vcoads}	COADS Latent Heat Flux
H_{Scoads}	COADS Sensible Heat Flux
τ_{xcoads} and τ_{ycoads}	COADS Stress components
$SST_c, AT_c, Q_c, W_c, UW_c$ and VW_c	Climatologies
L	Length scale
$\alpha, \beta, \gamma, \delta, \epsilon, \phi, \Gamma, \eta, \xi, \zeta, \rho, \Lambda, \mu, \nu, \sigma, \Pi, \Theta$	Coefficients
L	Length scale

The summation is over all points in space where the functional and gradient calculations can be computed. The functional is applied on a 2° by 2° grid over the Indian Ocean. The goal is to solve iteratively for SST, AT, Q, W, UW, and VW thereby indirectly solving for H, E, τ_x and τ_y . The Laplacian and curl terms provide curvature information as criteria and link the functional in space.

Each term in the functional is normalized by its standard deviation. The input fields are non-dimensionalized by their respective RMS basin-mean values in order to scale their magnitudes. Second-order finite differencing in spherical coordinates is used for all derivative calculations. The smoothing terms as well as the curl are non-dimensionalized by an appropriate length factor, L, which is chosen to be the grid spacing used in the finite difference operator. The length is 222.2 km. Furthermore, each grid point is logarithmically weighted according to the number of observations used in computing the monthly means.

The analysis is carried out for each of the 360 months of the 30-year period (January, 1960 through December, 1989). The COADS ship report fields are used as the first guess. If missing data exist in the first guess, climatology is used. Given the continental and island locations, the functional is evaluated at 888 locations on a 2° by 2° grid. The functional is solved for the six dependent variables. The interior continental boundary locations can not be evaluated for the Laplacian and curl terms. Moreover, two columns and rows along the perimeter of the analyzed region in the resultant fields are not considered since the functional is not completely defined at those and rows along the perimeter of the analyzed region in the resultant fields are not considered since the functional is not completely defined at those points. The total number of variables for which the gradient of the functional

is calculated is: $n = 6 \times 888 = 5328$. All other terms in the functional are functions of these six physical variables.

This method updates the flux fields at each iteration using the bulk formulae depending on changes in the resultant fields of the SST, AT, Q, W, UW and VW. Any alterations in these resultant fields can affect the other resultant fields through the flux constraint terms. For example, all drag coefficients in the bulk formulae are dependent on these fields. Similarly, a new saturated specific humidity field is calculated from updated SST fields at each iteration to provide a more accurate latent heat solution field.

Several techniques for determining the minimum of a functional were tested by Navon and Legler (1987). They found the conjugate gradient method to be most efficient when the number of parameters are large. The method produces a rapid reduction of the function by finding the gradient of the function with respect to the variables and combining the gradient with information from previous iterations. The specific algorithm used in this study is Conmin (Shanno and Phua, 1980). The Euclidian norm of the gradient must be reduced by nearly three orders of magnitude for convergence to occur. In this study, almost every analyzed month converged within 40 iterations or less.

3.2 Weight selection

The behavior of the functional and hence the solution fields are determined by the weights on each term of the functional. Empirical studies

The behavior of the functional and hence the solution fields are determined by the weights on each term of the functional. Empirical studies rather than truly objective means are used in selecting the optimal weights.

Objective methods for selecting the optimal weights are intractable due to the large number of variables solved in this study and are also difficult to use since an independent "truth" data set is difficult to obtain. Several criteria were used to determine the optimal weights: comparison of results to ship means at well sampled locations; qualitative comparisons of results to climatological studies (Hastenrath and Lamb, 1980 and Oberhuber, 1988); and a quantitative data void difference test.

Over 50 combinations of weights were tested for the months, August, 1965 and January, 1960 in order to determine the optimal weights. These months are used as representative of the summer and winter monsoon periods. A data void test was performed whereby input data for one $2^\circ \times 2^\circ$ grid point was removed and the analysis repeated. The difference between the objective results for different weight selections and the withheld data would ideally be minimal when the "correct" weights are used. The grid point (84°E , 4°N), just east of Sri Lanka was chosen because the area is rich with observations (75 observations in January, 1960 and 86 observations in August, 1965) and the withheld data are given more credence (based on sampling theory). The resultant values of the 10 surface variables at that station were compared to the values of the original data (Table 1).

For the final weights chosen, the pseudo-stress and wind stress values show the largest relative difference between the input and withheld values at the chosen grid point for January, 1960 more so than August, 1965. The zonal component of pseudo-stress and stress exhibit a larger difference in August because the direction of the winds are changing rapidly. The dramatic spatial component of pseudo-stress and stress exhibit a larger difference in August because the direction of the winds are changing rapidly. The dramatic spatial change in wind magnitude and direction contributes to a large difference in

Table 1. Quantitative error analysis of the 10 surface variables. One $2^\circ \times 2^\circ$ grid point at 84°E , 4°N , just east of Sri Lanka is withheld. The mean of all the surface parameters are shown for the withheld data. The difference between the final results when the grid point is withheld and the original data at that grid point is also given.

Surface Parameter	January 1960		August 1965	
	Mean of the withheld data	Difference between results and withheld data	Mean of the withheld data	Difference between results and withheld data
SST ($^\circ\text{C}$)	28.03	-0.02	27.87	-0.4
AT ($^\circ\text{C}$)	27.86	-0.12	27.65	-0.44
Q (g kg^{-1})	18.5	-1.0	19.1	-0.8
W (m s^{-1})	5.90	-0.9	8.70	-0.49
H (W m^{-2})	1.18	0.42	2.15	0.3
E (W m^{-2})	103.5	4.7	121.6	5.2
UW ($\text{m}^2 \text{s}^{-2}$)	-18.5	-6.24	69.0	9.76
VW ($\text{m}^2 \text{s}^{-2}$)	-23.1	5.31	41.2	-1.29
τ_x (N m^{-2})	-.14	-.07	.84	.17
τ_y (N m^{-2})	-.17	-.06	.50	.02

the error analysis. The wind flow changes from a nearly zonal flow around the Indian peninsula to southwesterly in the Bay of Bengal. In January, a sharp gradient in the magnitude of the pseudo-stress is observed near Sri Lanka. The direction is also changing from northeasterly to westerly.

Once the optimal weights were selected, several months' results were also examined for continuity between the input and resultant fields. The weight selection showed no seasonal dependence. Continuity is maintained regardless of season.

The optimal weights are shown in Table 2. The SST and AT terms are weighted more heavily than the other terms. If the temperature constraints are decreased, the fluxes degrade. The SST weight is more influential to the latent heat flux results than to the sensible heat flux results. The AT weight affects the sensible heat flux more than the latent heat flux as is expected. Larger constraints on Q also degraded the latent heat flux resultant field as well as the SST field.

The weight on the wind speed is significantly less than that of Legler (1992). The scalar wind field is analyzed as a variable in this study rather than as a function of the wind components as is done in Legler, 1992. Larger weights on W decrease the accuracy of the SST and heat flux fields.

The weights, ρ , Λ , μ , and ν act as smoothers for the resultant fields of SST, AT, Q , and W , respectively. The Laplacian terms couple the entire functional in space. The results are noisy without these terms. The Laplacian SST weight proved more influential than the weights on the other smoothing terms. Sensitivity analyses confirm this (section 5). The weight is larger than SST weight proved more influential than the weights on the other smoothing terms. Sensitivity analyses confirm this (section 5). The weight is larger than

the other Laplacian weights to insure the "smoothness" of the heat flux fields as well as the other fields.

The pseudo-stress winds and their Laplacian terms are all weighted at unity as are the stress terms. Stronger constraints on the pseudo-stress winds decrease the accuracy of the other fields and have very little effect on the pseudo-stress field. The curl of the pseudo-stress winds is weighted five times as large as these terms to approximate the expected wind derivative fields.

Table 2. The final weights for the functional terms are listed below.

Weight designator	Functional term	Value of the weight
α	Sea surface temperature	60.
β	Air temperature	20.
γ	Specific humidity	1.
δ	Scalar wind speed	5.
ϵ	Zonal pseudo-stress component	1.
ϕ	Meridional pseudo-stress component	1.
Γ	Sensible heat flux	.05
η	Latent heat flux	.5
ξ	Zonal stress component	1.
ζ	Meridional stress component	1.
ρ	SST smoothing term	10.
Λ	AT smoothing term	5.
μ	Q smoothing term	5.
ν	W smoothing term	5.
σ	UW smoothing term	1.
Π	VW smoothing term	1.
Θ	Curl of pseudo-stress winds	5.
Θ	Curl of pseudo-stress winds	5.

4. RESULTS

From the functional described in section 3, resultant fields of the 10 surface variables and fluxes are created for the 30-year period. The results are compared to independent data and demonstrate acceptable results. The solution fields of latent and sensible heat flux are especially accurate as is demonstrated in the sensitivity analysis (section 5).

The solution fields also contain the error estimates which are associated with the number of observations used to compute the monthly means. Each month contains r.m.s. error estimates in the 10 solution variables.

Finally, the variability of the fluxes is discussed. Annual and decadal variability is observed in the latent heat field through subjective and statistical analyses.

4.1 Monthly means

Comparisons between the input and resultant fields are shown to provide evidence as to the success of this study. For August 1965, the input SST field has a strong horizontal gradient in the southern Indian Ocean (Figure 3). In the north Indian Ocean, the SST is generally 27-28°C. This same distribution is observed in the resultant field of SST only much (Figure 5). In the north Indian Ocean, the SST is generally 27-28°C. This same distribution is observed in the resultant field of SST only much

smoother. The AT input also demonstrates a strong horizontal gradient off the western Australian coast. The values are 2-3°C cooler than the SST. Cooler air also prevails just off the coast of the Arabian peninsula. The resultant field of the AT (Figure 3) remains consistent to the input field. The north Indian Ocean AT is 27-28°C, but the southern Indian Ocean is as cool as 19°C.

In the Q field, the same strong horizontal gradient is observed in the southern Indian Ocean in the input and resultant fields (Figure 3). Values range from 9-18 g kg⁻¹. The weight on the "smoothing" term is five times as large as the weight on the input Q term. An accurate Q resultant field establishes greater confidence in the latent heat flux resultant field.

The seasonal wind flow patterns are detectable in the input W field. The strongest winds are observed in the Arabian Sea and in the southern trade wind belt as is expected during the summer monsoon (Figure 3). In the resultant field, the strongest speeds are also found in the Arabian Sea and in the trade wind belt, but they are more noticeable. The weakest winds exist over the equator between 50°E and 80°E.

The solution field of latent heat flux (Figure 4a), from August 1965, shows two maximums in the southern trade wind belt. The transfer is generally from the ocean to the atmosphere on a monthly scale. The resultant field of August, 1965 indicates this transfer. Minimum values are observed in the Bay of Bengal where weaker winds, high humidity and high temperatures are located. Off the coast of Somalia, latent heat flux is relatively high (120 W m⁻²). Again, the winds are strong in this region and temperatures are located. Off the coast of Somalia, latent heat flux is relatively high (120 W m⁻²). Again, the winds are strong in this region and tight gradients exist in the other surface fields.

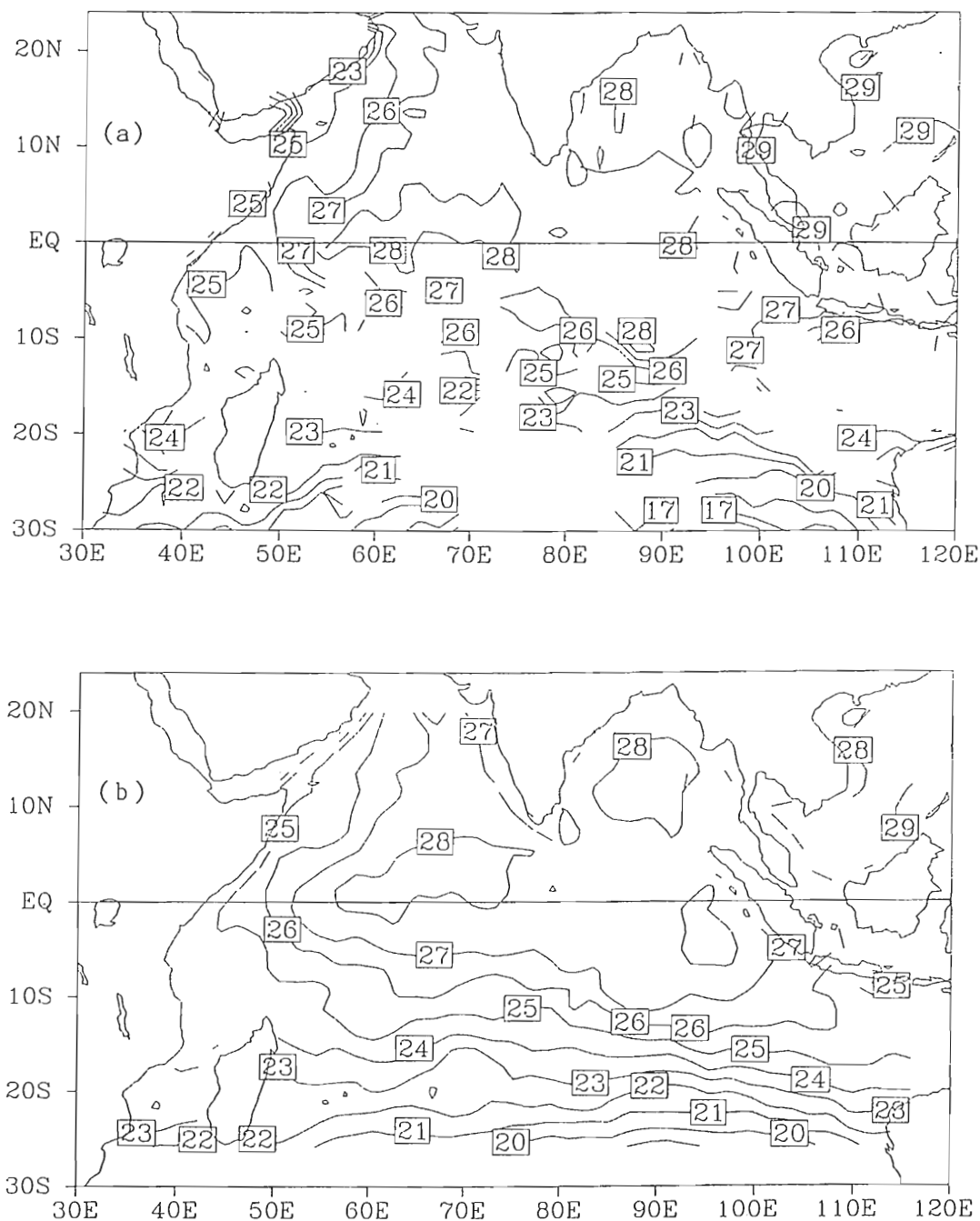


Figure 3. The input (top) and resultant fields (bottom) respectively of the surface variables using the optimal weights for the August 1965 case: (a-b) SST; (c-d) AT; (e-f) Q; (g-h) W; and (i-j) pseudo-stress vectors. Units are the same as in previous figures.

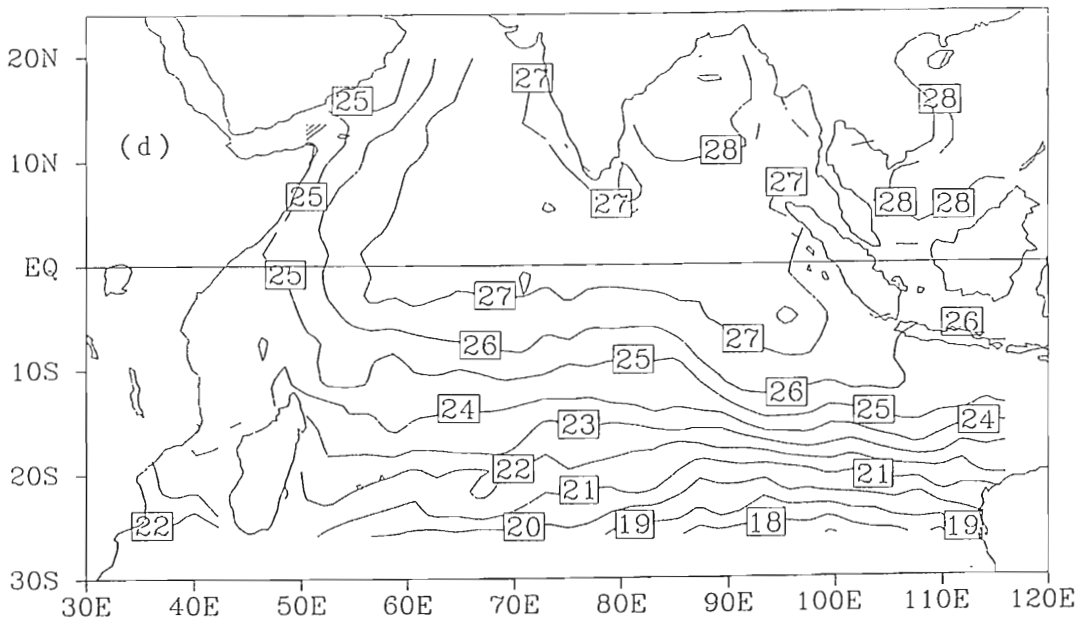
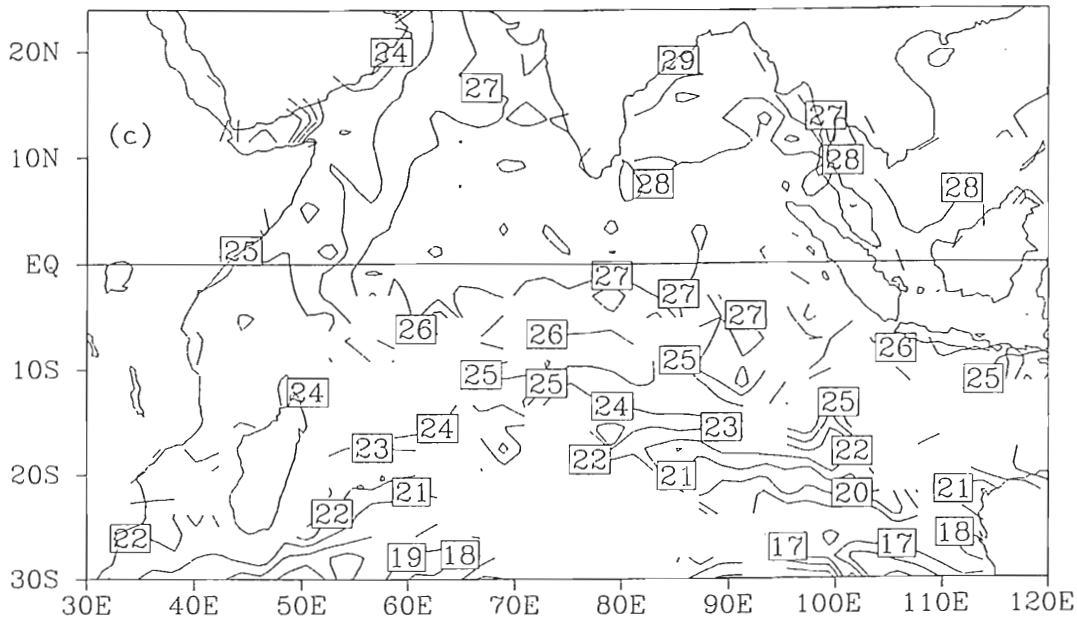


Figure 3. (Continued)

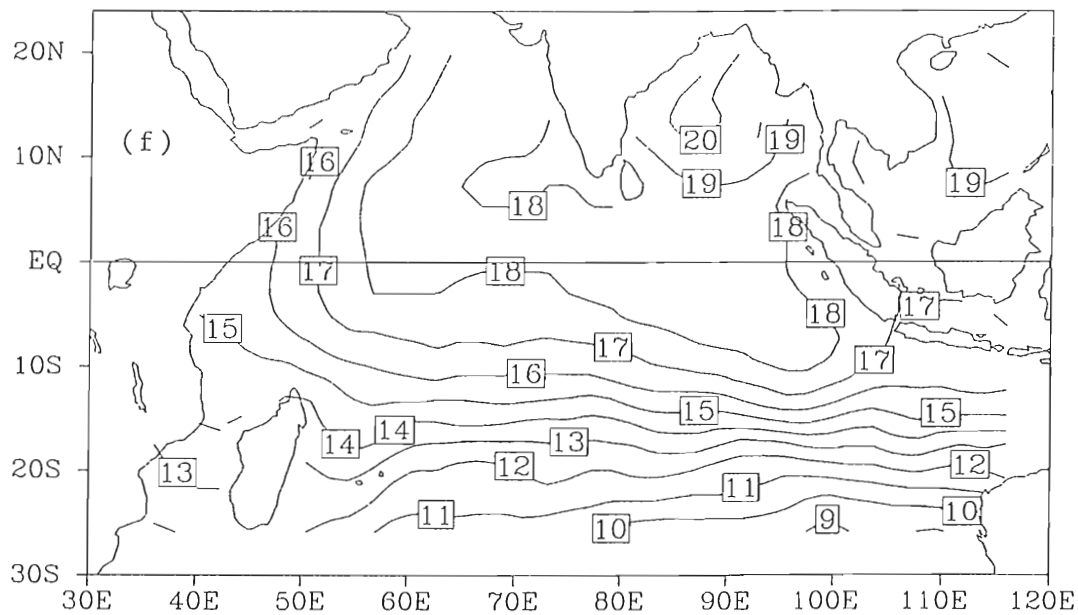
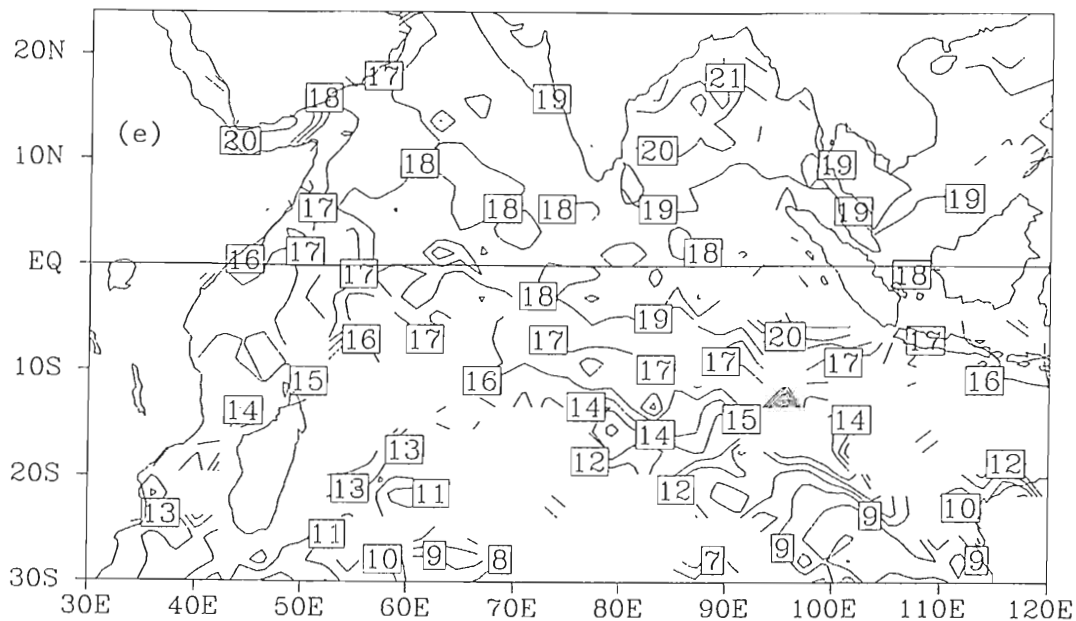


Figure 3. (Continued)

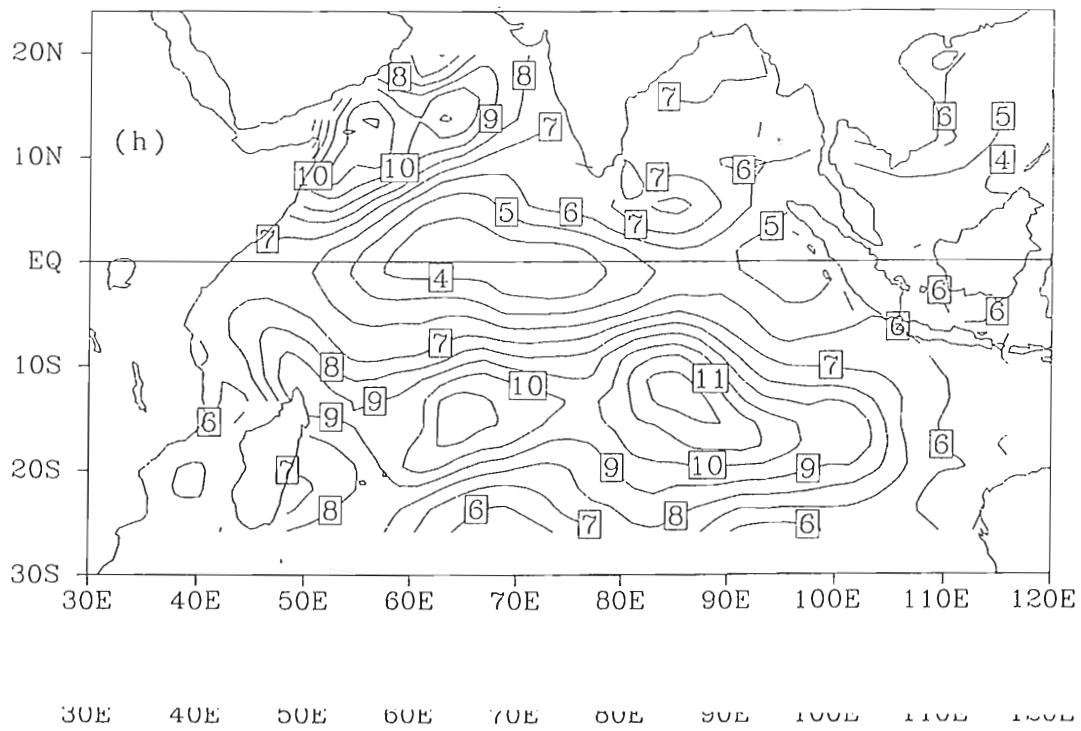
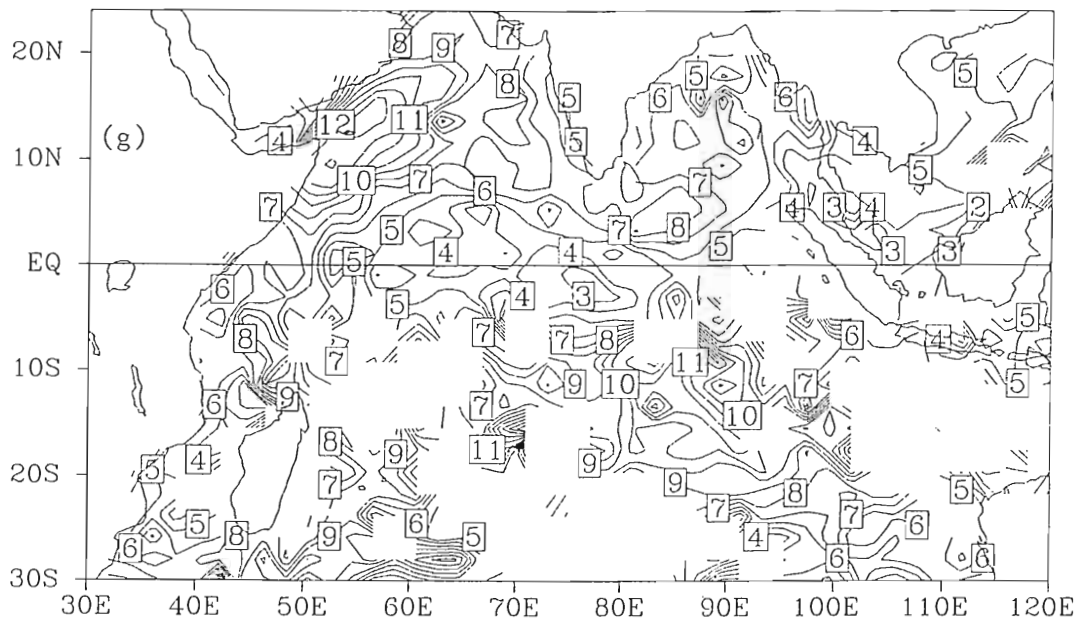


Figure 3. (Continued)

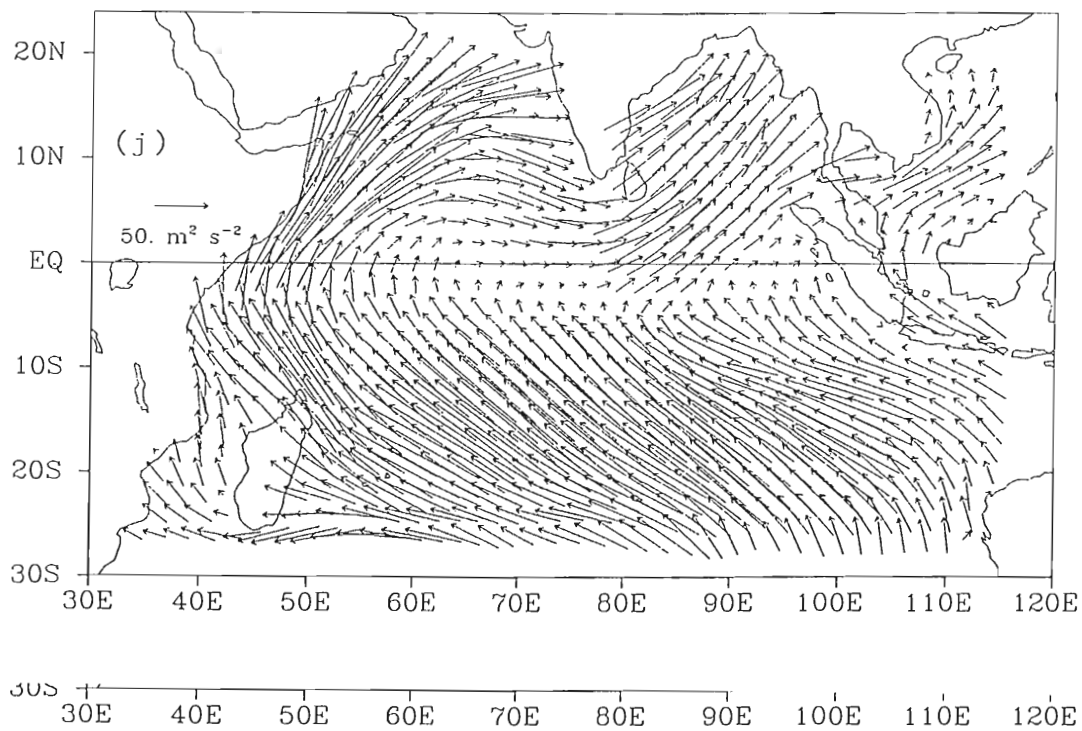
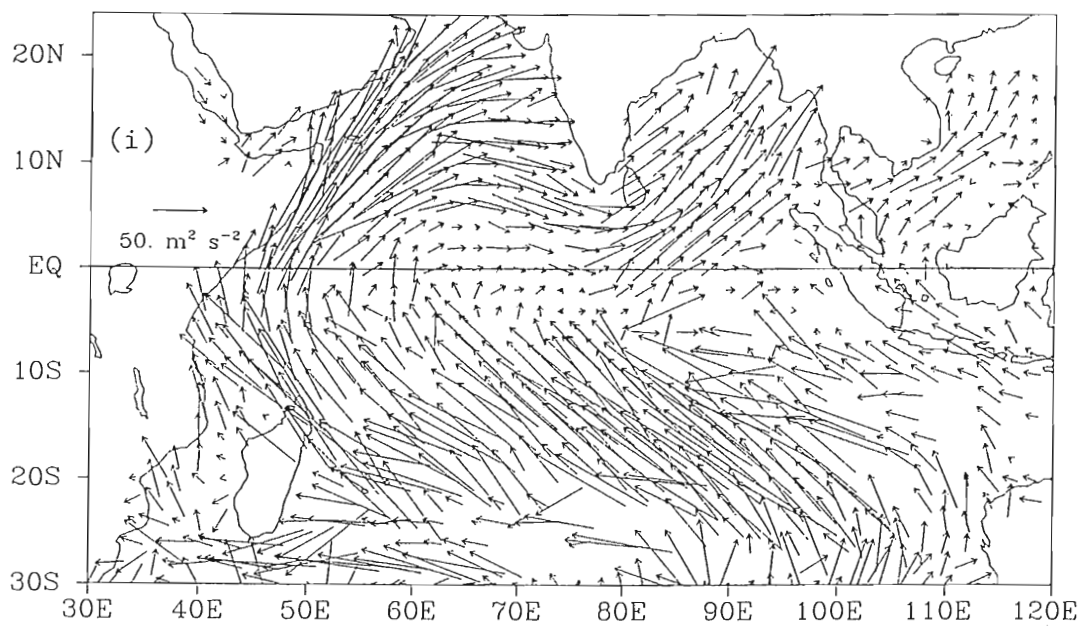


Figure 3. (Continued)

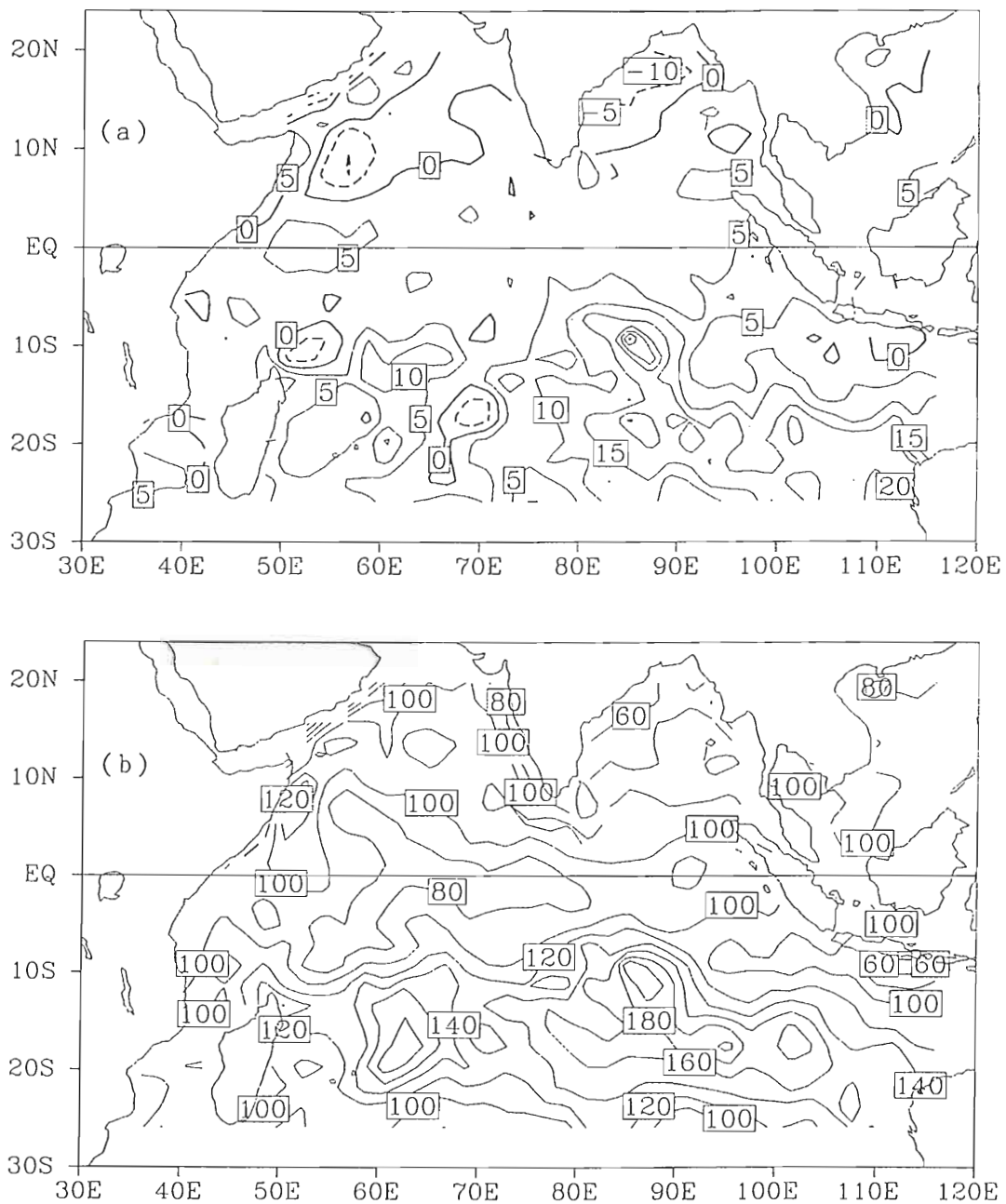


Figure 4. The resultant fields, using the optimal weights, of latent heat flux (a), sensible heat flux (b) and wind stress (c) for August 1965. Units are $W m^{-2}$ for heat fluxes and $N m^{-2}$ for wind stress.

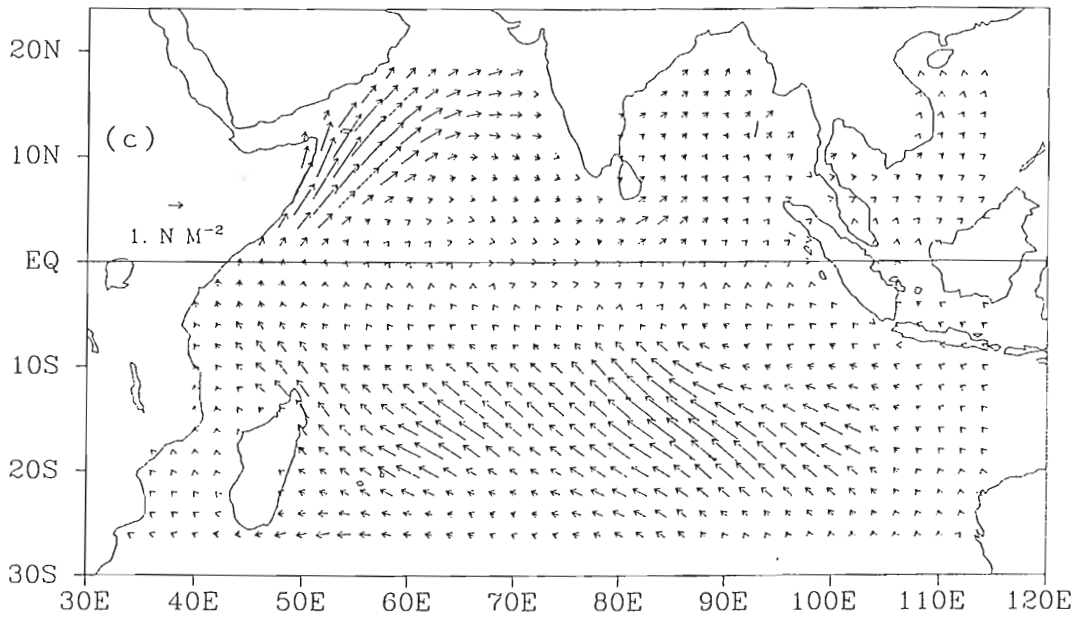


Figure 4. (Continued)

Figure 4. (Continued)

The sensible heat flux resultant field (Figure 4b) is somewhat noisy. The atmosphere transfers sensible heat to the ocean (negative values) off the eastern coast of India in the Bay of Bengal. Here, the difference in AT and SST is minimal. The wind speed is also weak which decreases the magnitude of sensible heat. Elsewhere, the ocean releases sensible heat into the atmosphere especially in the regions where the winds are strong and the difference in AT and SST are large, namely the southern trade wind belt.

Strong wind stress in the solution field for August 1965 is most prevalent in the southern trades and in the Arabian Sea as is expected during the southwest monsoon. The Intertropical Convergence Zone is observed along the equator.

4.2 Variability of the surface fluxes

Interannual, annual and decadal variability is observed in the surface fluxes. Variability is determined through subjective and statistical analysis (section 4.3). Several areas of significant variability include the Arabian Sea, the Bay of Bengal and the southern trade wind belt.

On an annual time scale, latent heat flux exhibits two maxima during July and August in the southern trade winds. Another secondary maximum is located in the Arabian Sea. Both areas are sustained by the strong summer monsoon. Maximum values of latent heat flux in the summer are generally 160 W m^{-2} in the trade winds and 120 W m^{-2} off the strong summer monsoon. Maximum values of latent heat flux in the summer are generally 160 W m^{-2} in the trade winds and 120 W m^{-2} off the Somali coast. The maximum in the Arabian Sea decreases westward as

evaporation is suppressed due to coastal upwelling (Surgi, 1990). As the northeast monsoon strengthens, latent heat flux exhibits maxima again in the Arabian Sea and in the southern trade winds just west of Australia. During the transition periods between the northeast and southwest monsoons, latent heat flux is considerably less than during the monsoon. In the north Indian Ocean latent heat flux is $60-80 \text{ W m}^{-2}$ and approximately 100 W m^{-2} in the trades during the spring and fall.

Sensible heat flux varies little in comparison to latent heat flux. Values are generally positive except where coastal upwelling occurs. The difference in the air-sea temperature exhibits the strongest influence on sensible heat flux. During the southwest monsoon, large positive values of sensible heat flux ($15-20 \text{ W m}^{-2}$) are observed off the western coast of Australia where the air-sea temperature difference is greater than 1°C . Smaller values are found in the north Indian Ocean where the temperature difference is negligible. During the northeast monsoon, sensible heat flux values range from $0-10 \text{ W m}^{-2}$ over the entire basin as air-sea temperature differences are insignificant. In the transitions periods, sensible heat flux varies even less than during the northeast monsoon, and values are in the range $\pm 5 \text{ W m}^{-2}$.

During the southwest monsoon, wind stress is large in the western Arabian Sea in association with the Findlater Jet. The trade winds in the Southern Hemisphere, west of 90°E , also exhibit large values of stress. Strong stress values are observed in the South China Sea during the northeast monsoon as a strong high pressure system builds over Asia. Strong stress values are observed in the South China Sea during the northeast monsoon as a strong high pressure system builds over Asia. Another high pressure system over Australia during the northeast

monsoon increases the stress in the trade wind region between 90-110°E. The transition periods show increased stress only in the southern trade winds.

Throughout the early 1960s, latent heat flux is higher in the Arabian Sea and the southern trade wind region near Madagascar. At the end of the 1960s and beginning of the 1970s, a decrease in latent heat flux is observed. A slight increase of latent heat flux is observed in the Arabian Sea beginning in the middle 1970s. The 1980s depict a 15% increase ($\sim 20 \text{ W m}^{-2}$) in latent heat flux from the 1960s. A similar trend is observed in the wind speed and wind stress over the Arabian Sea. Higher wind speeds produce more evaporation and turbulent mixing which is transported from the Southern Hemisphere trades into the Arabian Sea (Cadet and Diehl, 1984).

Both the Arabian Sea and the trade wind region near Madagascar experience lower SST when the winds are stronger and latent heat flux larger. These results agree with the findings of Joseph and Pillai (1984) and Krishnamurti (1981). The SST in the middle of the Arabian Sea does not decrease as significantly as the SST along the Saudi Arabian and Somali coasts does during a wet southwestern monsoon. Stronger winds drive Ekman pumping (Dube *et al.*, 1990) and strong coastal upwelling decreases the SST. McCreary and Kundu (1989) consider the Arabian Sea SST to be more influenced by the upwelling near the coasts and the offshore advection. Evaporative heat flux due to increased wind is considered secondary. However, this study concludes that the wind speed rather than the SST over the Indian Ocean is more influential to latent heat flux secondary. However, this study concludes that the wind speed rather than the SST over the Indian Ocean is more influential to latent heat flux (Figures 5 and 6).

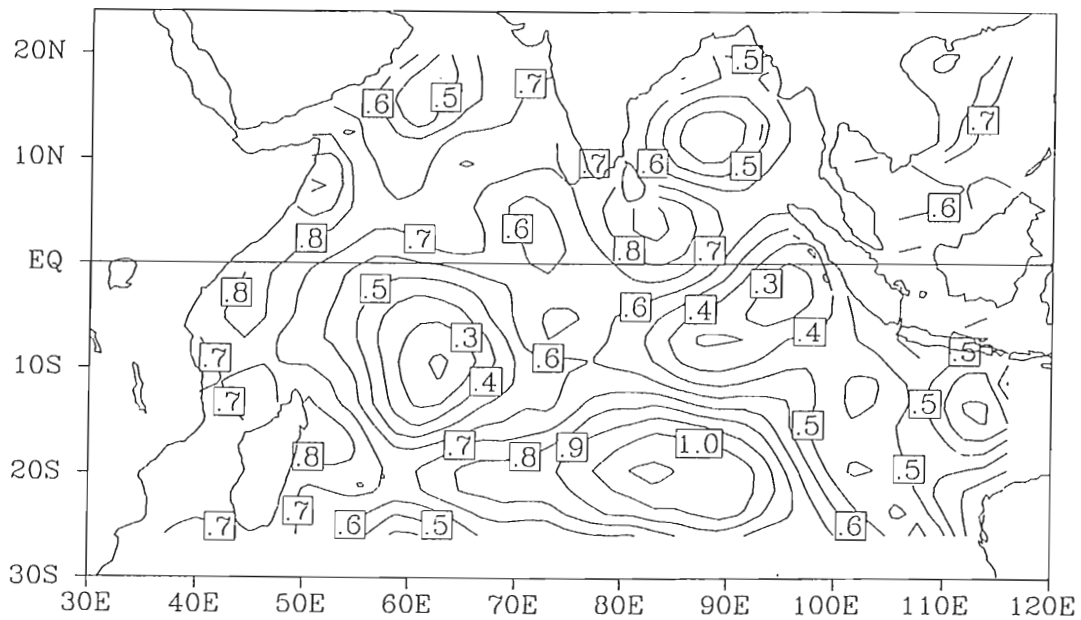


Figure 5. The difference in the average wind speed of the sixties and the eighties is shown. Contour intervals are $.1 \text{ m s}^{-1}$. The largest difference between the decades are observed in the trade winds and along the Somali coast. Minima are found at 10°S near Madagascar and at the equator near Sumatra.

winds and along the Somali coast. Minima are found at 10°S near Madagascar and at the equator near Sumatra.

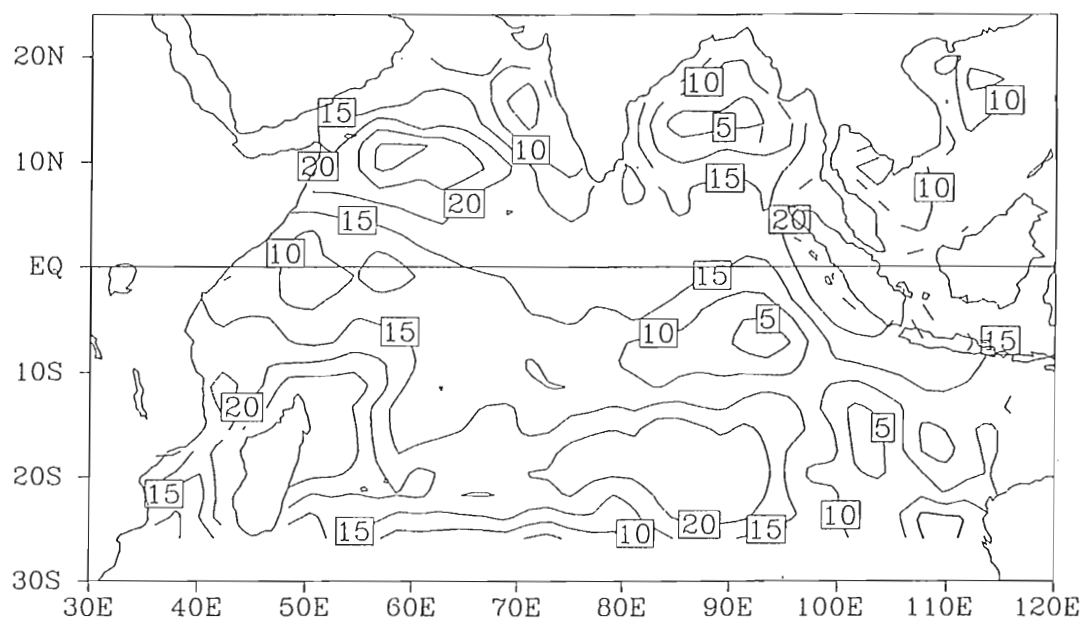


Figure 6. The difference in the average latent heat flux in the sixties and the eighties is shown. Contour intervals are in 5 W m^{-2} . The largest differences are observed in the trade winds and in the Arabian Sea. The maximum differences in the latent heat correspond to the maximum differences in wind speed shown in figure 5.

the trade winds and in the Arabian Sea. The maximum differences in the latent heat correspond to the maximum differences in wind speed shown in figure 5.

In the Bay of Bengal, higher values of latent heat flux are observed during the dry southwest monsoon years of 1965, 1979, 1982, and 1985 (Shukla, 1987 and Parthasarathy *et al.*, 1990). Conversely, lower values of latent heat flux are found during the years of higher rainfall over India. As the Bay of Bengal is on the leeward side of India during the strong southwest monsoon, precipitation due to evaporative flux in India diminishes slightly before reaching the Bay of Bengal. Latent heat flux is still relatively high in the Bay of Bengal during a wet monsoon, but the values are significantly less than those in the Arabian Sea.

Although the Bay of Bengal monsoon is significantly less in strength than the Arabian monsoon, the same relationship between the wind speed and latent heat flux observed in the Arabian Sea exists. In addition, the SST in the Bay of Bengal is higher than anywhere else in the Indian Ocean.

The negative correlation between the SST and wind speed noted previously and described by Shukla (1987) is not as prominent in the Bay of Bengal. Coastal upwelling is minimal here compared to the Arabian and Somali coasts. When coastal upwelling occurs off of India in the Bay of Bengal, sensible heat flux is negative. However, for the 30-year period of discussion, sensible heat flux is predominantly positive.

The eastern portion of the Southern Hemisphere trade wind belt (80°E to Australia) demonstrates an opposing view of conditions in the Arabian Sea. Higher values of latent heat flux are noticed in the early sixties and in the late eighties. A notable decrease exists from 1967 to 1973. The same prerequisites for higher latent heat flux exist for the Arabian Sea and off of the late eighties. A notable decrease exists from 1967 to 1973. The same prerequisites for higher latent heat flux exist for the Arabian Sea and off of Australia. Higher winds and wind stress provide higher evaporative flux.

Lower AT and SST also exist. However, the years which show the strongest latent heat flux off Australia are the same years that latent heat flux is minimal in the Arabian Sea and vice versa.

Sensible heat flux in the eastern trade wind belt is always positive. Higher values of sensible heat flux are located in the years of the dry Indian southwest monsoon. The SST and AT differ greatly ($\sim 1^\circ\text{C}$) during these years.

4.3 EOF Analysis

An EOF analysis is performed on the resultant fields of latent heat flux and wind stress to examine further their variability. The spatial and temporal variability of latent heat flux and wind stress are linked in this statistical analysis which partitions the variance of the fluxes. An EOF analysis of sensible heat flux is unnecessary as the variance is small compared to the variance of latent heat flux. The resultant fields contain 745 stations over the Indian Ocean for the 360 months due to the boundary conditions imposed on the functional (section 3). Temporal means of the latent heat and wind stress components are removed initially to insure that the largest eigenmode is not the mean pattern.

For latent heat flux, the first eigenmode accounts for 26% of the total variance. This mode physically describes the fluctuations in the latent heat flux in relationship to the wind field during the southwest monsoon. A 12-month moving average of the time series closely resembles the interannual flux in relationship to the wind field during the southwest monsoon. A 12-month moving average of the time series closely resembles the interannual latent heat flux variability noted previously in the Arabian Sea (section 4.1).

A small trend, $.23 \text{ W m}^{-2} \text{ year}^{-1}$, in the first eigenmode is related to a similar trend in the scalar wind ($.05 \text{ m s}^{-1} \text{ year}^{-1}$). This trend is the result of climatic change or instrument bias. The time series shown (Figure 7a) removes the trend in order to examine more completely the variability of latent heat flux. The raw time series of latent heat flux, however, demonstrates a trend of $10 \text{ W m}^{-2} \text{ decade}^{-1}$ in the Arabian Sea, the South China Sea and in the southern trades.

Combining the spatial pattern (Figure 7b) with the time series for this first mode, strong latent heat flux anomalies are noted in the north Indian Ocean. The spatial pattern is dominated by the Findlater Jet in the Arabian Sea. Large decadal variability is observed in the time series of latent heat flux. Lower evaporation is noted during the 1960s. The 1970s exhibit a biannual oscillation similar to the monsoon signal during the decade (Parthasarathy, *et al.* 1990). The middle 1980s demonstrate a decrease in latent heat flux. Three dry monsoon periods occurred between 1984 and 1987. Not only does the first EOF mode correlate well to the monsoon signal, large decadal variability is observed.

Joseph, *et al.* (1991) allude to the relationship between the Indian summer monsoon rainfall and El Niño events. However, the relationship is small and results are inconclusive. However, they found more correlation between the Australian summer monsoon and El Niño. Rasmusson and Carpenter (1983) find a relationship among higher SSTs in the eastern and central equatorial Pacific Ocean, positive pressure anomalies over the Indian Ocean and a weaker southwest monsoon. The extremely dry central equatorial Pacific Ocean, positive pressure anomalies over the Indian Ocean and a weaker southwest monsoon. The extremely dry monsoons which led to severe droughts in India over the period 1975-1979

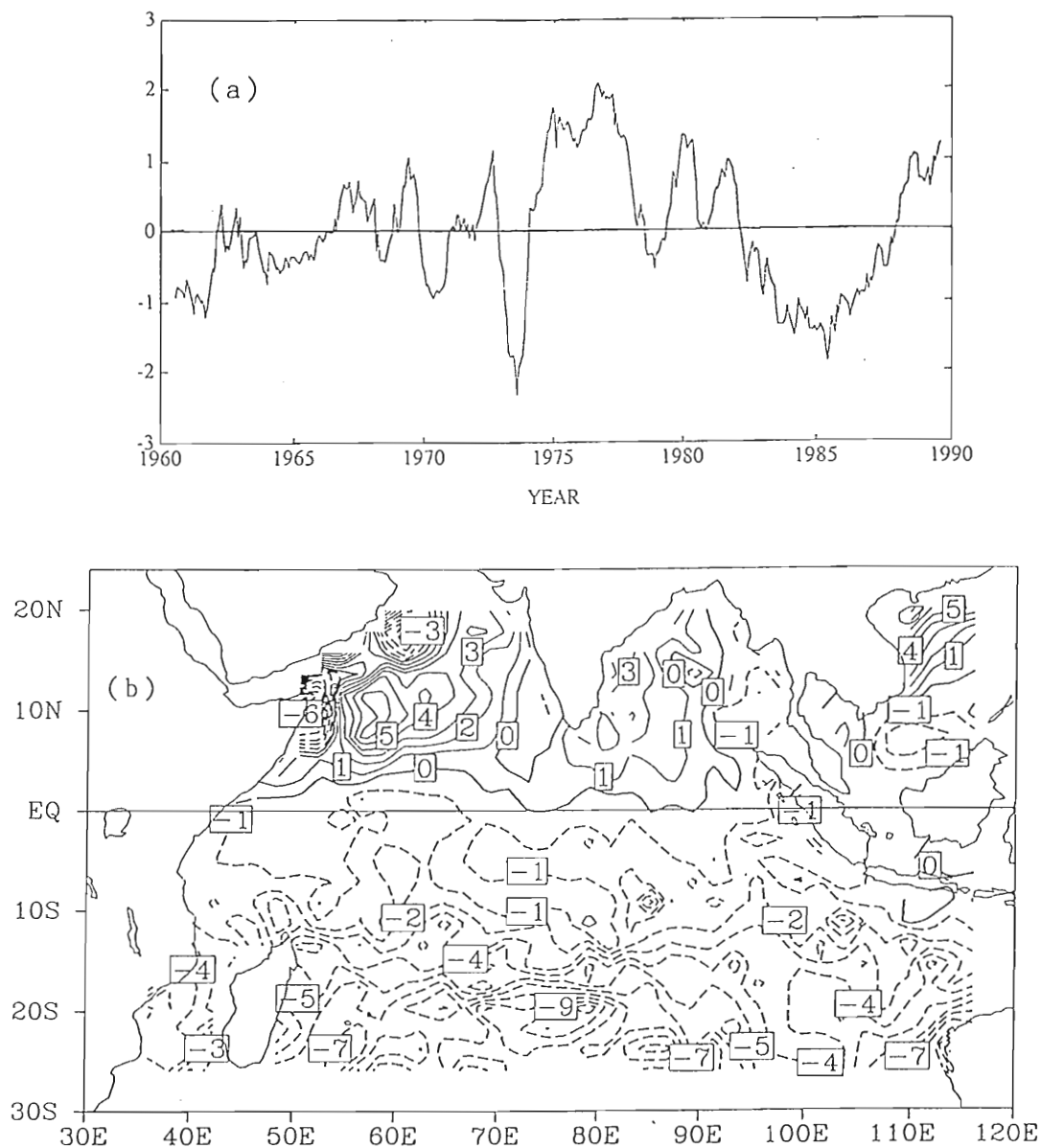


Figure 7. (a) Time series of the first eigenvector of latent heat flux with a 12-month moving average. Discrepancies in the time series are due to the fact that the onset of the Indian summer monsoon does not contain a perfect annual signal. (b) The spatial pattern of the first eigenmode of latent heat flux. Contour series are due to the fact that the onset of the Indian summer monsoon does not contain a perfect annual signal. (b) The spatial pattern of the first eigenmode of latent heat flux. Contour intervals are in 1 W m^{-2} . The first mode represents 26% of the total variance.

corresponded to only 20% of the warm El Niño years. Meanwhile, 40% of the El Niño years were accompanied by a relatively dry monsoon. The EOF analysis shows no correlation between latent heat flux over the Indian Ocean and El Niño.

The second eigenmode accounts for 11% of the variance. The variability of the northeast monsoon is most prevalent in this mode, particularly the South China Sea region. Another slight trend in the latent heat flux is observed ($.17 \text{ W m}^{-2} \text{ year}^{-1}$) in relation to the trend in the scalar wind speed ($.05 \text{ W m}^{-2} \text{ year}^{-1}$). The remaining eigenmodes account for equal portions of the variance and are considered noise.

Vector EOF analysis (Legler, 1989) is performed on the wind stress components. The temporal means of the wind components are initially removed. The magnitude and phase of the wind stress are used to physically interpret the results. The first eigenmode accounts for 73% of the total variance. The time series indicates the variation of the summer and winter monsoons. The summer monsoon is more variable than the winter monsoon. The time series (Figure 8a) indicates a trend ($.005 \text{ N m}^{-2} \text{ year}^{-1}$) which begins in the middle 1970s. This trend is attributed to the increase in the wind speeds in Arabian Sea (section 4.1) during the southwest monsoon and in the South China Sea during the northeast monsoon. Anomalously high values of wind stress (Figure 8b) are observed in the Arabian Sea, Bay of Bengal and the South China Sea. The spatial pattern represents the wind stress field during the southwest and northeast monsoons and contains a phase of $\pm 180^\circ$. These summer and winter months experience the most stress field during the southwest and northeast monsoons and contains a phase of $\pm 180^\circ$. These summer and winter months experience the most variability on an annual scale.

The second eigenmode accounts for 6% of the total variance of wind stress. The transitional periods are represented in this mode as only the variance in the trade winds are observed. The remaining modes contain equal portions of the variance and as with the remaining modes in the latent heat flux, they can not be examined independently.

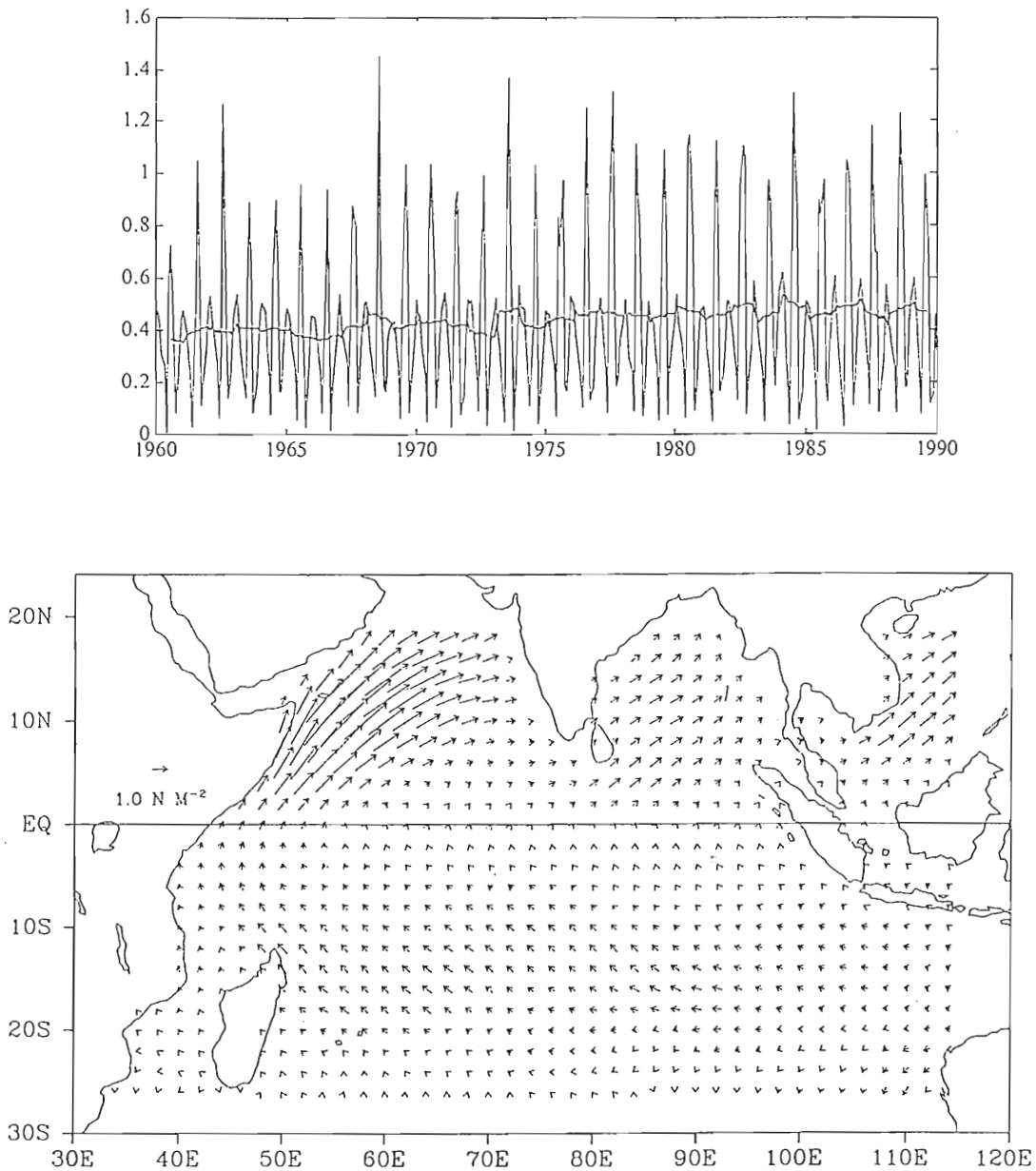


Figure 8. (a) The time series of the first eigenvector of the wind stress, corresponding to 73% of the variance. The 12-month moving average is superimposed (thicker line) to indicate the trend. Discrepancies in the moving average are due to the fact that the onset of the Indian summer monsoon does not have a perfect annual signal. (b) The spatial structure of the first eigenmode of wind stress. Contour intervals are $.05 \text{ N m}^{-2}$.

5.0 SENSITIVITY ANALYSIS

A sensitivity analysis is performed on each of the weights in the functional which affect the resultant fields of latent heat flux and the magnitude of wind stress. A first-order finite difference method detailed by Cacuci (1988) is used to test the sensitivity. The goal is to ascertain the change in the selected response functions for a prescribed change in the optimal weights. The response function should be a simple function of the solution. Any number of response functions can be chosen. For this study, a function describing the total latent heat flux and the total magnitude of stress over all points in space is used.

Absolute sensitivity describes the change in the total response function for a certain change in the weights. The relative sensitivity is the normalized absolute sensitivity and aids in determining the regions which are most affected by a change in the optimal weights. The response functions for latent heat flux (R_E) and wind stress ($R_{\vec{\tau}}$) are defined as:

$$R_E = \sum_{ij} E_{ij}$$

and

$$R_{\vec{\tau}} = \sum_{ij} \left(\tau_{x(ij)}^2 + \tau_{y(ij)}^2 \right)^{\frac{1}{2}} .$$

ij

The relative sensitivities (S_r) of latent heat flux and wind stress to a certain weight, α , in the functional are defined as such:

$$S_{r(E)} = \frac{\alpha}{R_E} * \frac{\partial R_E}{\partial \alpha}$$

$$S_{r(\tau)} = \frac{\alpha}{R_\tau} * \frac{\partial R_\tau}{\partial \alpha}$$

Each weight from the set of optimal weights (Table 3) is altered $\pm .5\%$ for a total change of 1%. The functional is then recalculated with the altered weights to determine the relative sensitivity in the response functions.

For the optimal weights, all except the Laplacian term for the SST indicate less than a 1% change in the response functions of latent heat and wind stress for a 1% change in each weight. Both response functions are more sensitive to the weights on the SST, scalar wind and their "smoothing" term counterparts. The response function of the wind stress is more sensitive to these weights than the latent heat flux. The wind stress is also more sensitive to the weights on the Laplacian terms of the pseudo-stress components.

The local sensitivity error locates the regions in which the actual resultant fields of latent heat flux and wind stress are most affected by a prescribed change in the optimal weights. It is similar to an r.m.s. error in the resultant fields. Local sensitivity error (L_s) of the latent heat flux is defined:

$$L_s = \left[\frac{1}{17} \sum_{k=1}^{17} (E_{ij} - E_{ij}(k*10\%))^2 \right]^{\frac{1}{2}} .$$

$$L_s = \left[\frac{1}{17} \sum_{k=1}^{17} (E_{ij} - E_{ij}(k*10\%))^2 \right]^{\frac{1}{2}} .$$

A similar equation is used for wind stress by replacing the change in latent heat flux with the change in the magnitude of the wind stress. The change implied above represents the difference in the resultant field of the latent heat flux using the optimal weights and the latent heat flux fields when the 17 optimal weights are adjusted to 10 times their relative sensitivities as given in Table 3. For a 10% change in the relative sensitivities, the r.m.s. error in the latent heat field due to the relative uncertainties in all of the optimal weights is given in terms of the local sensitivity error (Figure 7a). The largest error is $\pm 20 \text{ W m}^{-2}$. Latent heat flux is most affected in the region of the Somali Jet, the Bay of Bengal and off the western coast of Australia where the trade winds are strong. In these regions during August, latent heat flux is on the order of 240 W m^{-2} . These results support the relationship between the latent heat flux and scalar wind field.

Local sensitivity of wind stress is concentrated in the trade winds and in the western Arabian Sea (Figure 7b). Variation in the Somali Jet affect the amount of coastal upwelling present and the strength of the wind. The SST and wind speed have the highest relative sensitivities (Table 3) to the wind stress because they are meteorologically significant in these areas. Local sensitivity errors are as high as $.2 \text{ N m}^{-2}$.

Table 3. The relative sensitivities of the optimal weights which influence the latent heat flux and wind stress. The values are given for August 1965. All other months are similar. A 1% change in the weights in the first column yields the percentage change listed for the latent heat flux and wind stress response functions.

Functional Term Weights	$S_r(E)$	$S_r(\tau)$
α	-.026	.52
β	-.00008	-.0007
γ	-.0004	-.0001
δ	.0047	.0012
ϵ	.0003	-.0005
ϕ	.0006	-.0005
ρ	.049	-1.07
Λ	.0029	.006
μ	.0076	.005
ν	-.027	-.127
σ	.01	-.487
Π	.01	-.488
Γ	-.005	.007
η	.001	-.016
ξ	-.0018	.0018
ζ	-.0039	.006
Θ	-.0039	.016

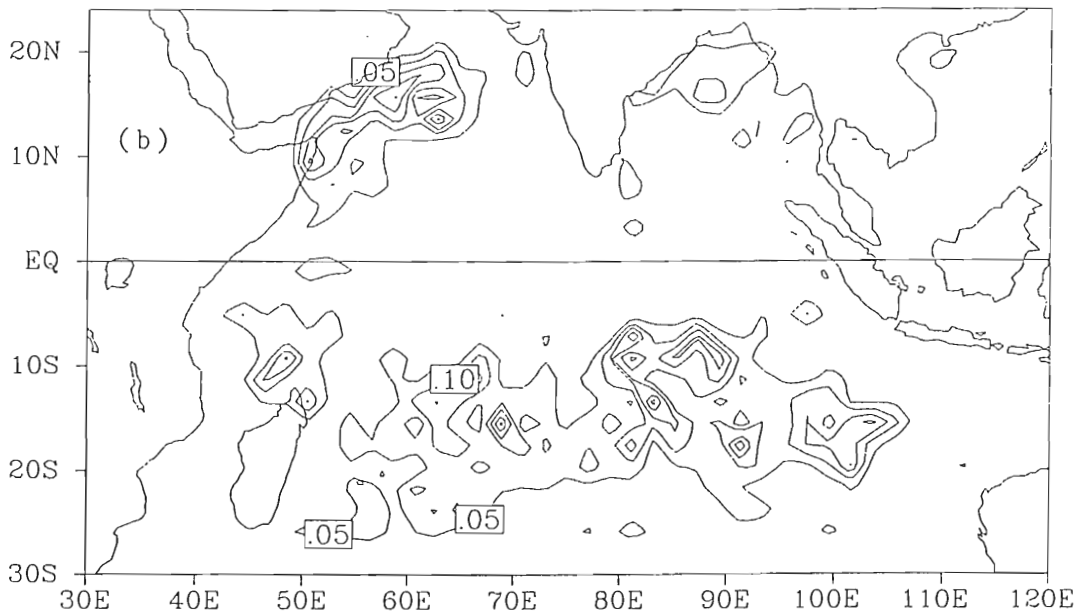
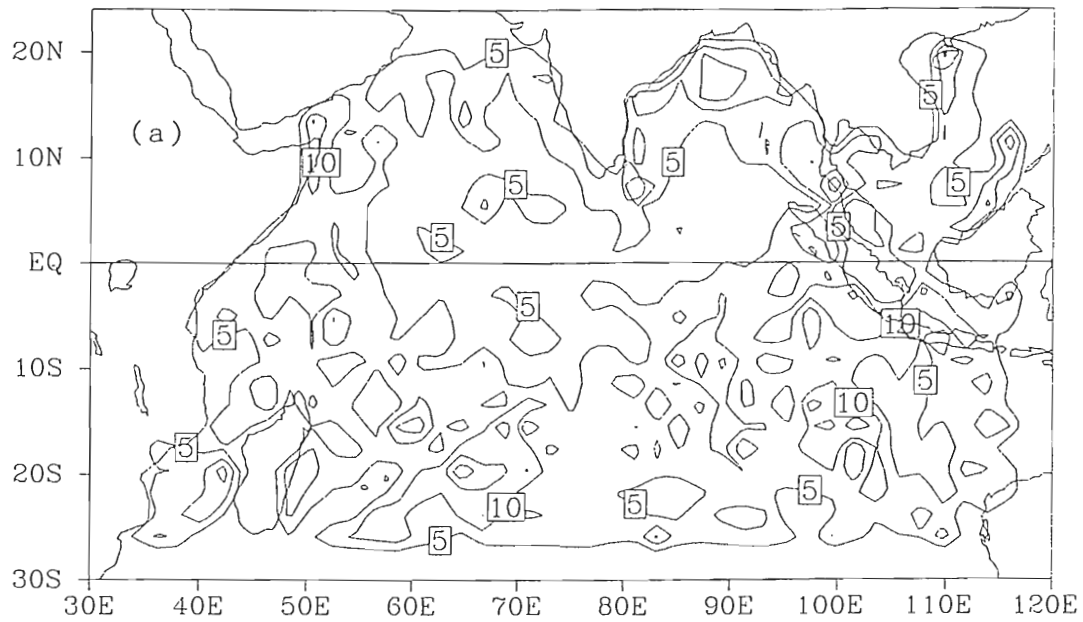


Figure 8. The local sensitivity of (a) latent heat flux and (b) wind

Figure 8. The local sensitivity of (a) latent heat flux and (b) wind stress due to the relative uncertainty of the optimal weights. Contour intervals are 1 W m^{-2} for latent heat flux and $.05 \text{ N m}^{-2}$ for wind stress.

6. CONCLUSIONS and SUMMARY

A consistent set of monthly mean maps of surface variables and fluxes over the Indian Ocean are created simultaneously using a variational-direct minimization objective analysis technique. The surface fluxes are coupled to and determined by the surface variables. The input data are from COADS ship reports for the 30 year period, 1960-1989. A longer period could be examined if enough data are available.

The optimal weights are selected by comparison of the results to ship means at well sampled locations, a qualitative comparison of the results to previous studies and through a quantitative data void test described in section 3. The first-order finite difference method of sensitivity described in section 5 allows one to narrow the focus of the results to certain weights. This sensitivity analysis was not previously performed in other studies. It is important to note that sensitivity analysis can be performed on functions with a large number parameters. The solutions of latent heat flux and wind stress are more sensitive to the weights on the SST and W terms. These terms exhibit more annual variability especially along the African coastline and in the Arabian Sea.

Once the solution fields are created for the entire period, the variability of the fluxes are examined. On a monthly time scale, the transport of latent heat is always from the ocean to the atmosphere. The latent heat flux is most of the fluxes are examined. On a monthly time scale, the transport of latent heat is always from the ocean to the atmosphere. The latent heat flux is most influenced by the wind. The SST exerts a secondary influence in the regions

of coastal upwelling. Meanwhile, areas of high wind speed such as the southern trade winds and the Arabian Sea generate larger values of latent heat flux by pumping more moisture from the Southern Hemisphere into the Northern Hemisphere during the southwest monsoon. Therefore, the relationship of stronger wind speed, higher latent heat flux and more precipitation over India is established. During the northeast monsoon, latent heat flux is transferred into the south Indian Ocean from the north Indian Ocean. The largest values of latent heat flux and precipitation are observed over the islands of Borneo and Java and in the northwestern regions of Australia.

The trade wind region near Australia is particularly interesting in relation to the monsoon. During the dry monsoon years over India, the southern trade winds between 80°E and 110°E are stronger than normal and the latent heat flux is anomalously large. A negative correlation could be further proven with Australian rainfall data.

Wind stress exhibits large annual variability depending on the wind speed during the monsoon. Little decadal variability is observed other than a slight trend which is also noted in the wind speed.

The EOF analyses of latent heat flux and wind stress support the findings in section 4.2. The lack of variability in the wind stress is confirmed. Large decadal variability in latent heat is observed in associations with the Indian summer monsoon rainfall. Surprisingly, no relationship exists between latent heat flux and El Niño. A definite relationship is established between Indian rainfall and latent heat flux. Given Australian rainfall data, between latent heat flux and El Niño. A definite relationship is established between Indian rainfall and latent heat flux. Given Australian rainfall data,

a relationship between latent heat flux and Australian rainfall could provide a link to El Niño.

Meteorological implications of the surface fluxes over the Indian Ocean are discovered. This information concerning the variability of latent heat flux in relation to surface parameters such as wind speed, SST, AT and humidity can be utilized more extensively in future Indian Ocean models.

7. APPENDIX

Monthly mean results

Analysis results of the surface variables and surface fluxes for a typical January (1976) and July (1984) are shown in figures 9-10. The differences in the parameters during the southwest and northeast monsoons are evident.

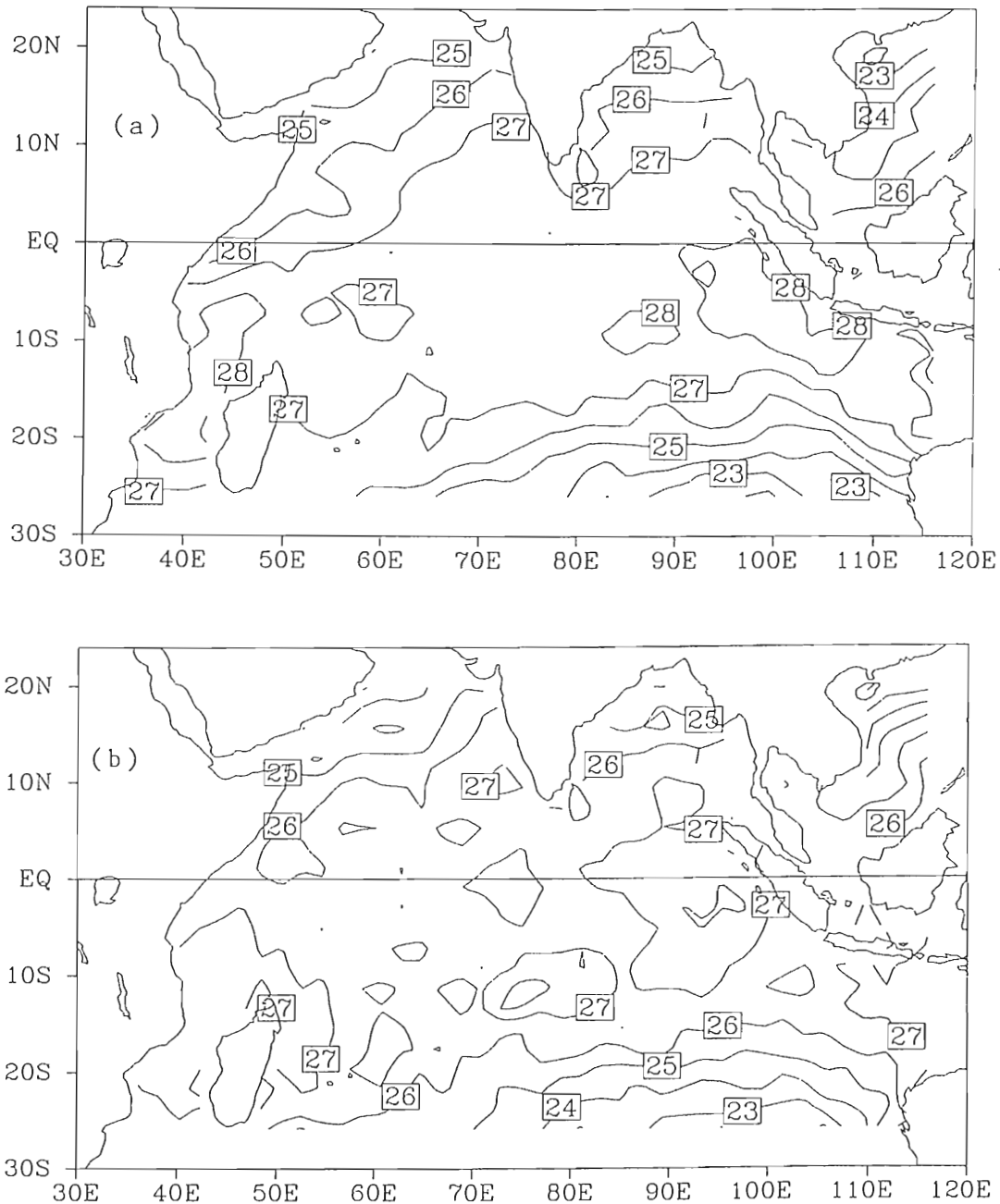


Figure 10. Monthly means resultant fields for January 1976 are shown: (a) SST; (b) AT; (c) Q; (d) W; (e) latent heat flux; (f) sensible heat flux; (g) pseudo-stress vectors and (h) wind stressvectors. The units are the same as in previous figures. During January, the wind speed is stronger in the South China Sea and the southern trade winds. Latent heat flux is large in these areas as well.

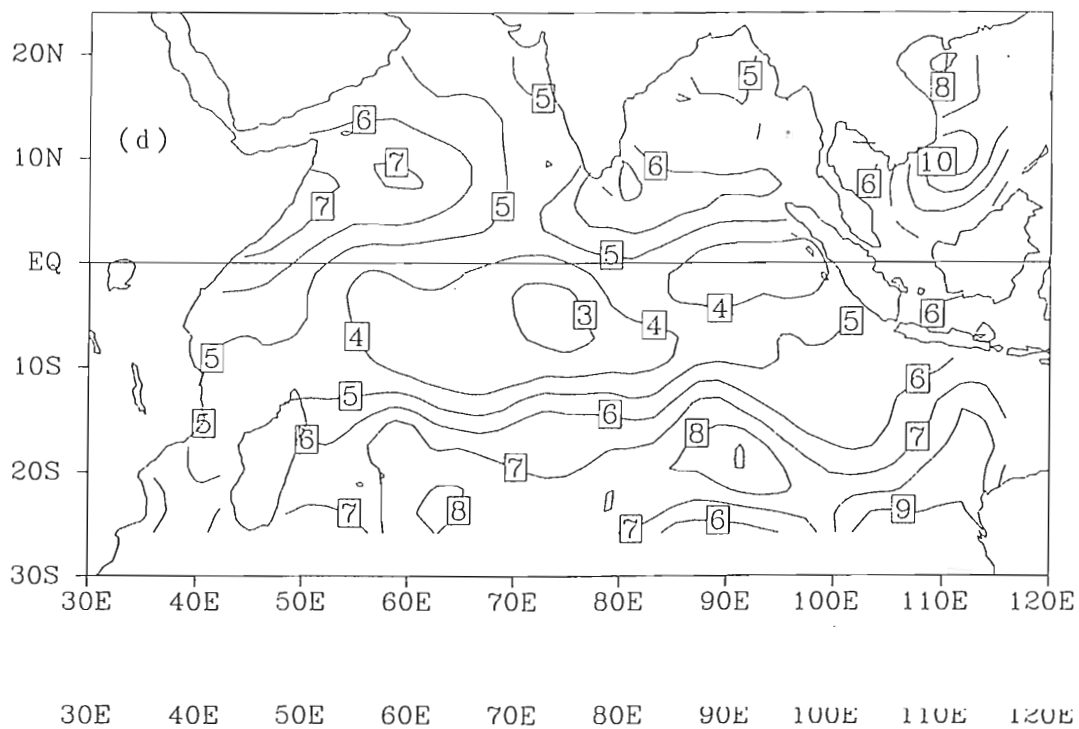
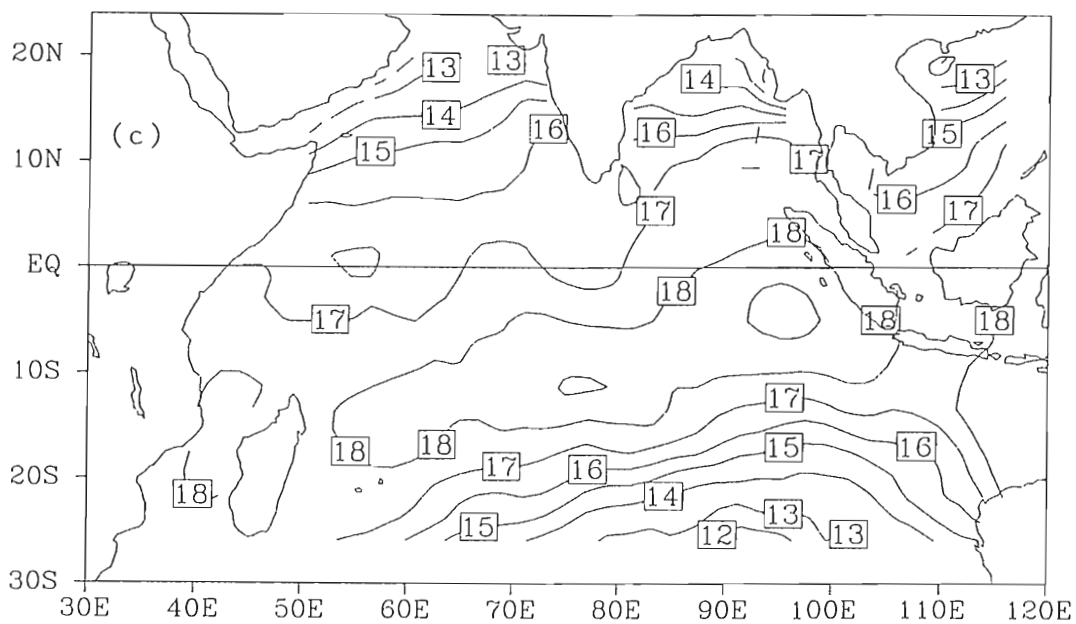


Figure 10. (Continued)

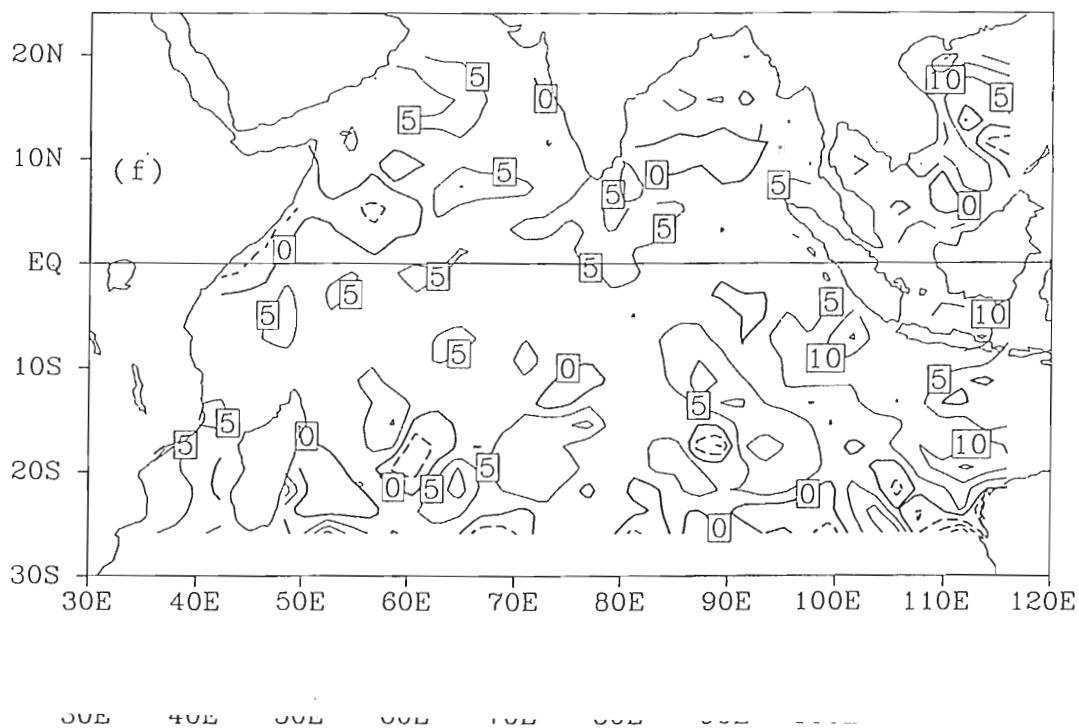
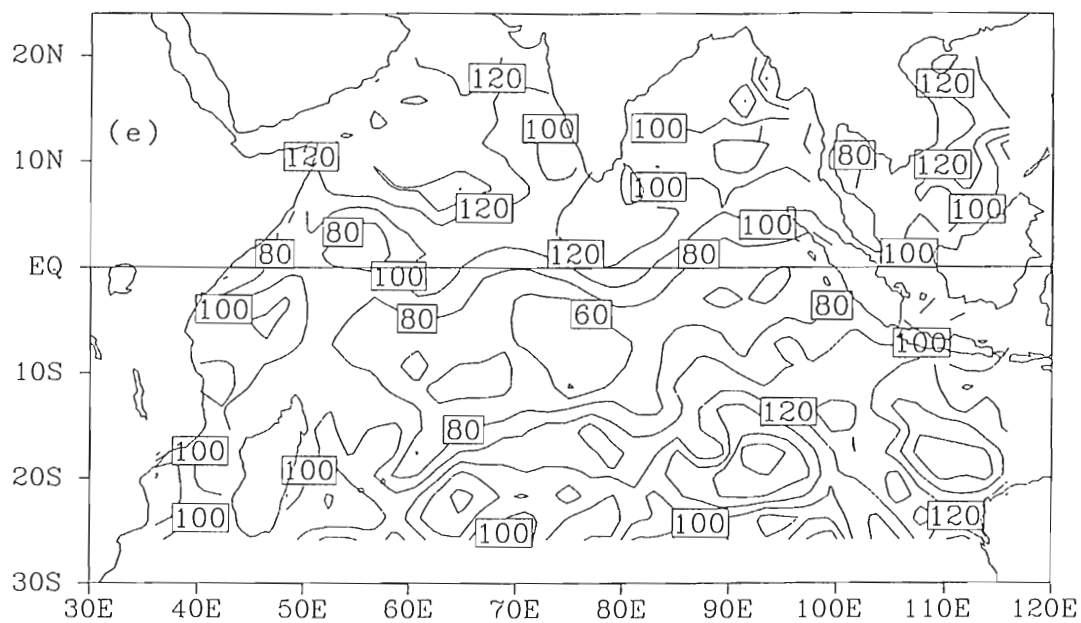


Figure 10. (Continued)

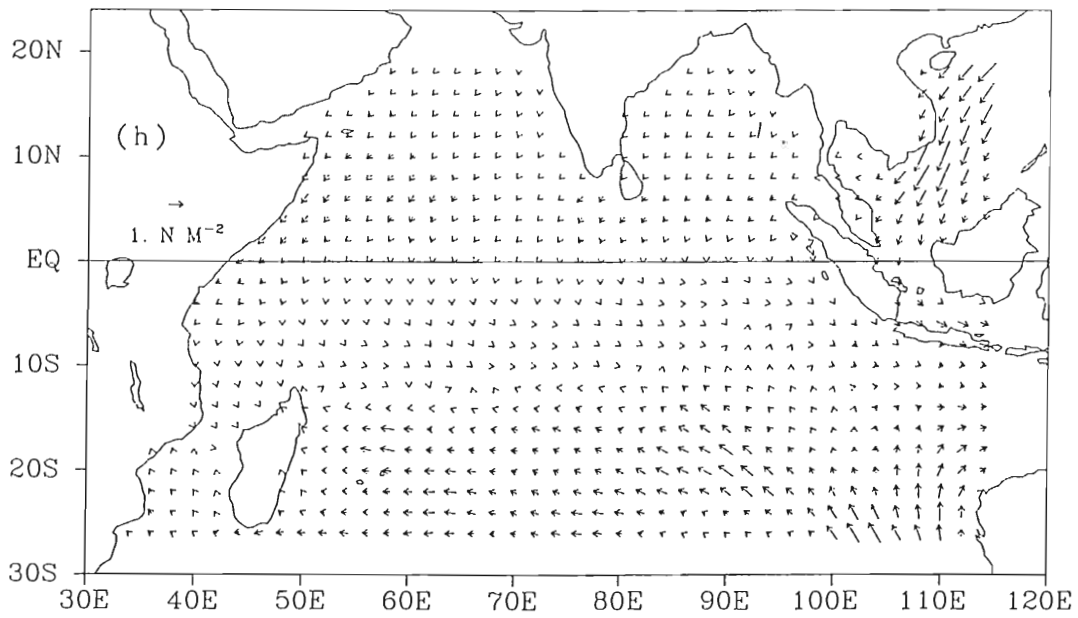
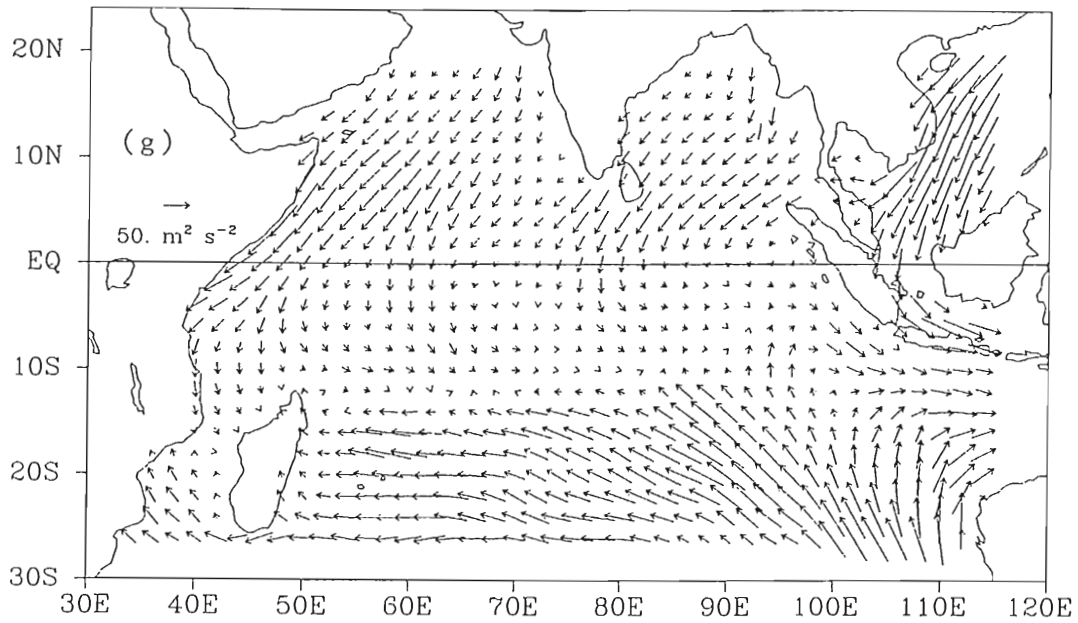


Figure 10. (Continued)

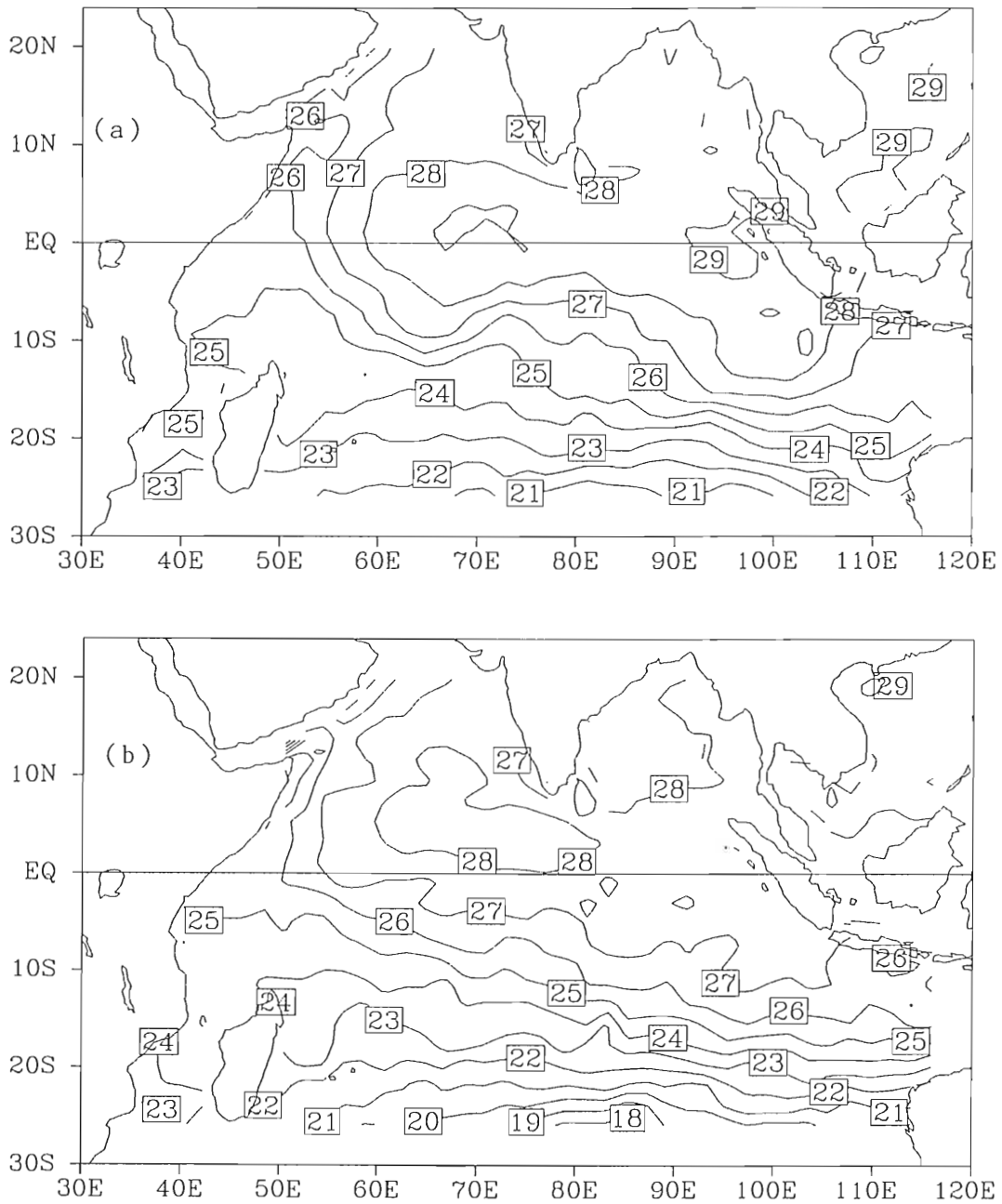


Figure 11. Monthly mean resultant fields are shown for July 1984: (a) SST; (b) AT; (c) Q; (d) W; (e) latent heat flux; (f) sensible heat flux; (g) pseudo-stress vectors and (h) wind stress vectors. Units are the same as in previous figures. The Indian summer 1984: (a) SST; (b) AT; (c) Q; (d) W; (e) latent heat flux; (f) sensible heat flux; (g) pseudo-stress vectors and (h) wind stress vectors. Units are the same as in previous figures. The Indian summer monsoon is observed in the strong wind speeds over the Arabian Sea. The SST and Q are higher during July in the north Indian Ocean. A maximum of latent heat flux is observed in the trade winds.

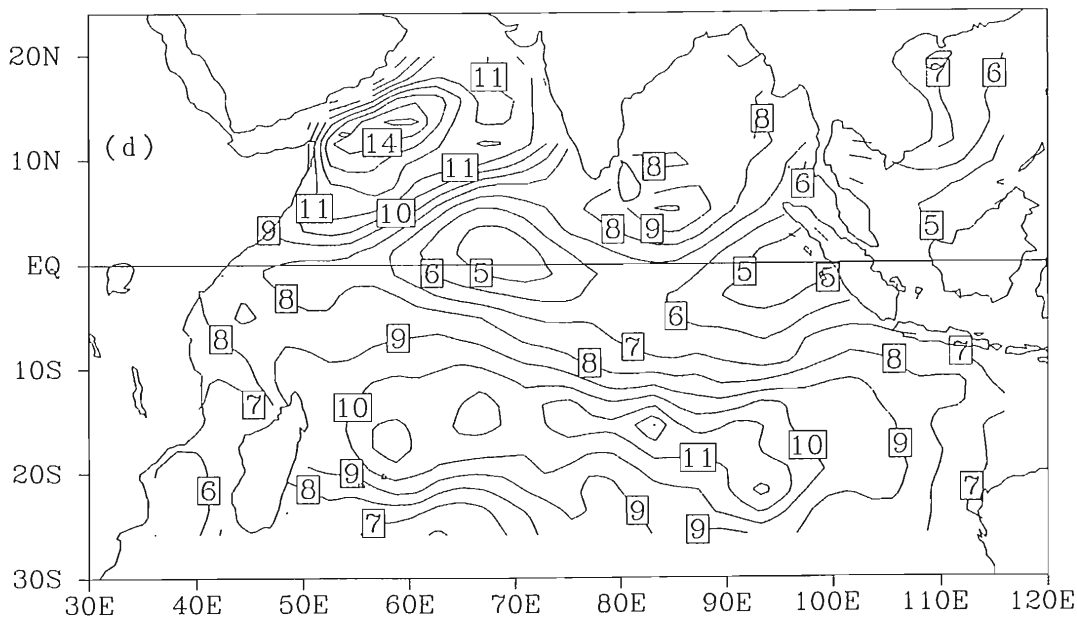
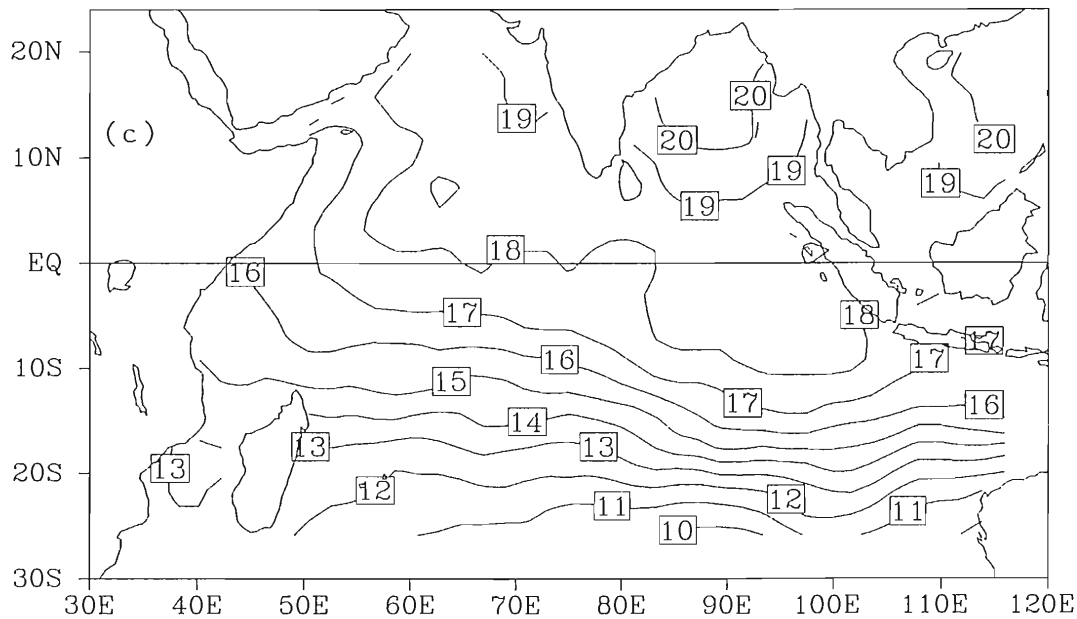


Figure 11. (Continued)

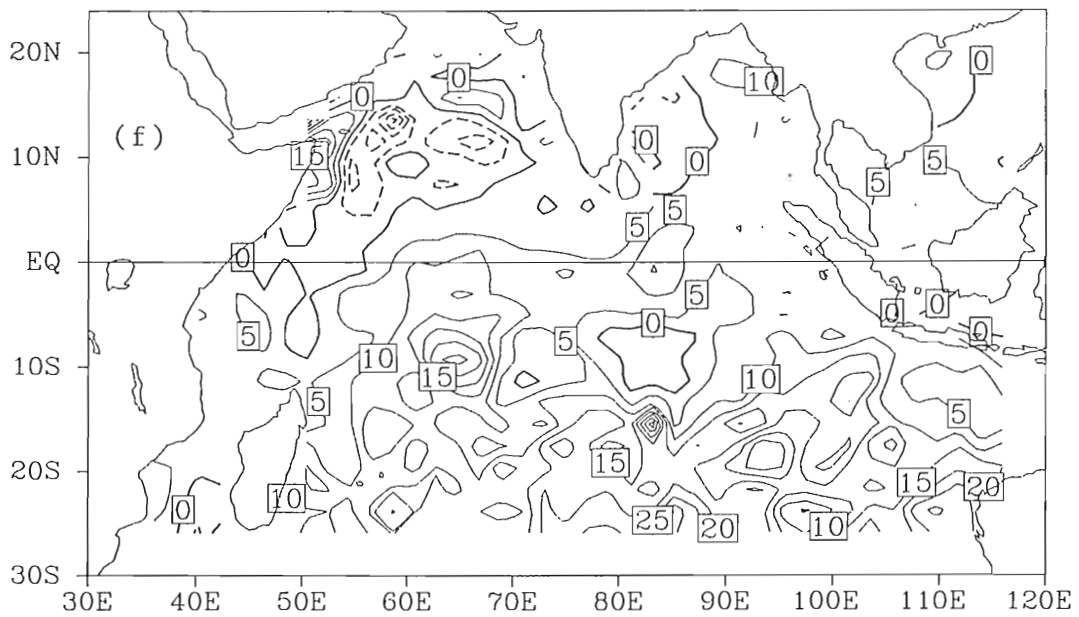
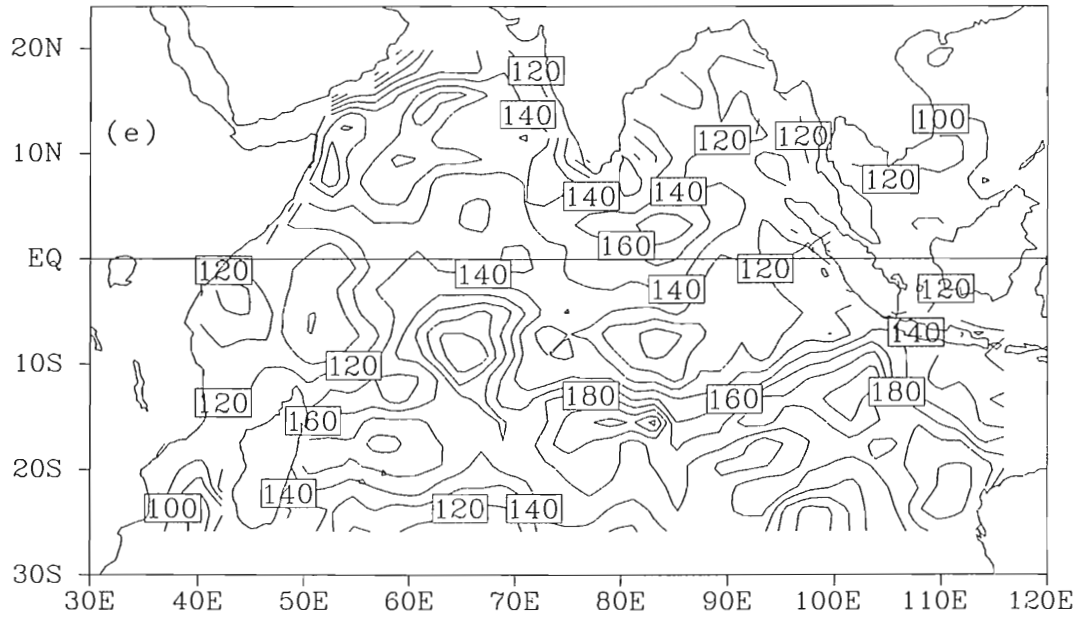


Figure 11. (Continued)

Figure 11. (Continued)

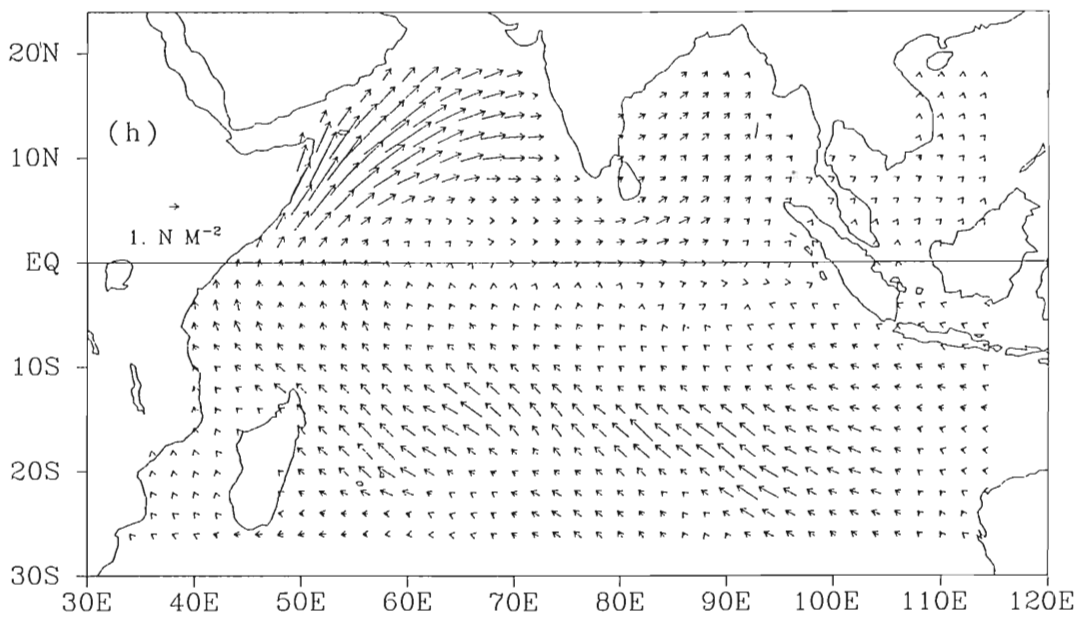
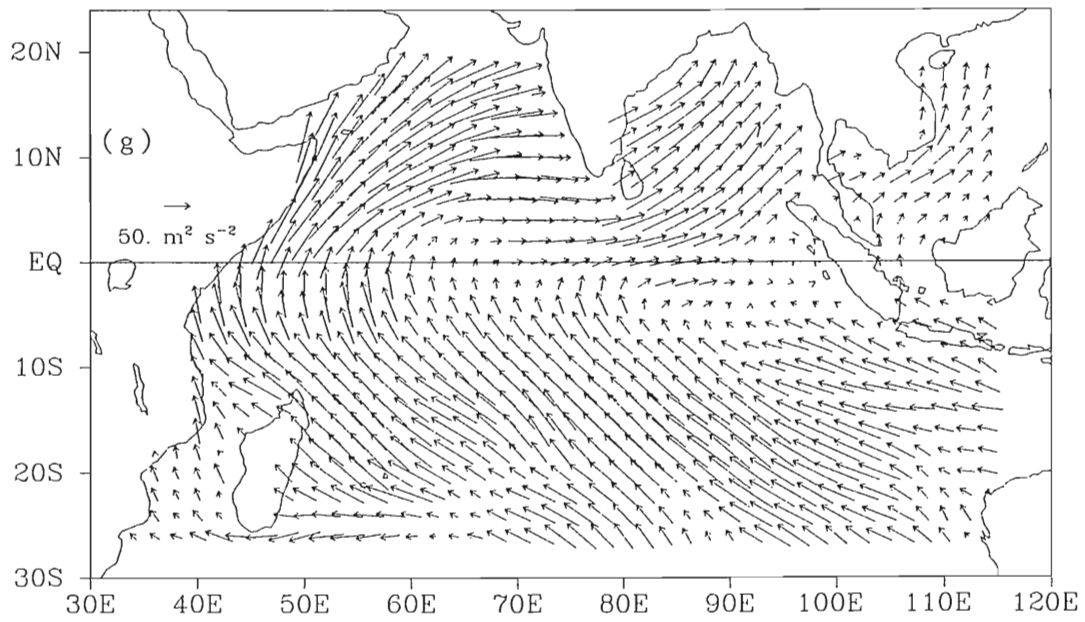


Figure 11 (Continued)

Figure 11. (Continued)

References

- Cacuci, Dan G., 1988: The forward and adjoint method of sensitivity analysis. In: Ronen, Y. (Ed.) *Uncertainty Analysis*, Boca Raton, Florida: CRC Press, Inc., 282pp.
- Cadet, Daniel L. and Bradley C. Diehl, 1984: Interannual variability of surface fields over the Indian Ocean during recent decades, *Monthly Weather Review*, October, **112**, pp. 1921-1935.
- Cayan, D.R., 1990: Variability of latent and sensible heat fluxes over the oceans. *Ph D. Dissertation*, University of California, San Diego, 199pp.
- Congbin, Fu, Zhang Mingli, Joseph Fletcher, Su Binkei and Quan Xiaowei, 1990: Atlas of climate physics of Tropical Pacific Ocean. Science Press, Beijing, China, 190pp.
- Dube, S. K., M. E. Luther and J. J. O'Brien, 1990: Relationships between interannual variability in the Arabian Sea and Indian Summer Monsoon Rainfall, *Meteorology and Atmospheric Physics*, **44**, pp. 153-165.
- Esbensen, Steven K., and Richard W. Reynolds, 1981: Estimating monthly averaged air-sea transfers of heat and momentum using the bulk aerodynamic method, *Journal of Physical Oceanography*, **11**, pp. 457 - 465.
- Frankignoul, C. and R.W. Reynolds, 1983: Testing a dynamical model for mid-latitude sea surface temperature anomalies, *Journal of Physical Oceanography*, **13**, pp. 1131-1145.
- Hanawa, K. and Y. Toba, 1987: A new analysis of monthly mean wind stress over the global ocean, Department of Atmospheric Sciences, Oregon State University, Report No. 26, 148 pp.
- Haney, R.L., 1985: Midlatitude sea surface temperature anomalies: a numerical hindcast, *Journal of Physical Oceanography*, **15**, pp. 787-799.
- Haney, R.L., 1985: Midlatitude sea surface temperature anomalies: a numerical hindcast, *Journal of Physical Oceanography*, **15**, pp. 787-799.

- Hastenrath, Stefan and Peter J. Lamb, 1979: Climatic Atlas of the Indian Ocean, Part I: Surface climate and atmospheric circulation, The University of Wisconsin Press, 100pp.
- Hastenrath, S. and P. J. Lamb, 1980: On the heat budget of the hydrosphere and atmosphere in the India Ocean, *Journal of Physical Oceanography*, **10**, pp. 694 - 708.
- Hoffman, Ross N., 1984: SASS wind ambiguity removal by direct minimization. Part II: Use of smoothness, *Monthly Weather Review*, **112**, pp. 1829-1852.
- Hsiung, Jane, 1986: Mean surface energy fluxes over the global ocean, *Journal of Geophysical Review*, **91**, pp. 10,585 - 10,606.
- Joseph, P.V. and P.V. Pillai, 1984: Air-sea interaction on a seasonal scale over north Indian Ocean-Part I: Interannual variations of sea surface temperature and Indian summer monsoon rainfall, *Mausam*, **35**, pp. 323-330.
- Joseph, P.V., B. Liebmann and H.H. Hendon, 1991: Interannual variability of the Australian Summer Monsoon onset: Possible influence of Indian summer monsoon and El Niño, *Journal of Climate*, **4**, pp. 529-538.
- Knox, Robert A., 1987: The Indian Ocean: Interaction with the monsoon. In: Fein, J. S., Stephens, P. L. (Eds.) *Monsoons*, New York: John Wiley & Sons, 632 pp.
- Krishnamurti, T.N., 1981: Cooling of the Arabian Sea and the onset-vortex during 1979. Recent progress in equatorial oceanography. A report of the final meeting of SCOR working group 47 in Venice, NOVA University, NYIT Press.
- Kumar, M. R. Ramesh and L. V. Gangadhara Rao, 1990: Annual mean statistics of the surface fluxes of the tropical Indian Ocean, *Boundary Layer Meteorology*, **51**, pp. 299-312.
- Large, W. G. and S. Pond, 1982: Sensible and latent heat flux measurements over the ocean, *Journal of Physical Oceanography*, **12**, pp. 464 - 482.
- Legler, David M., 1983: Empirical Orthogonal Function analysis of wind vectors over the Tropical Pacific Region, *Bulletin of the American Meteorological Society*, **64**, pp. 234-241.
- Legler, David M., 1983: Empirical Orthogonal Function analysis of wind vectors over the Tropical Pacific Region, *Bulletin of the American Meteorological Society*, **64**, pp. 234-241.

- Legler, David M., I. M. Navon and James J. O'Brien, 1989: Objective analysis of pseudostress over the Indian Ocean using a direct-minimization approach, *Monthly Weather Review*, **117**, pp. 709-720.
- Legler, David M., 1992: Analysis of air and sea physical properties and surface fluxes using a combination of in-situ and SEASAT data, *Ph.D. Dissertation*, Florida State University, 135pp.
- McCreary, J.P. and P.K. Kundu, 1989: Numerical investigation of sea surface temperature variability in the Arabian Sea, *JGR-Oceans*, **94**, C11, pp. 16,097-16,114.
- Navon, I. M. and David M. Legler, 1987: Conjugate-Gradient methods for large-scale minimization in meteorology, *Monthly Weather Review*, **115**, pp. 1479 - 1502.
- Oberhuber, Josef M., 1988: An atlas based on the 'COADS' Data Set: The budgets of heat, buoyancy and turbulent kinetic energy at the surface of the global ocean, Max-Planck Institut für Meteorologie, Hamburg, Germany, 100pp.
- Parthasarathy, B. and D. A. Mooley, 1978: Some features of a long homogeneous series of Indian summer monsoon rainfall, *Monthly Weather Review*, **106**, pp. 771-781.
- Parthasarathy, B., N.A. Sontakke, A.A. Monot and D.R. Kothawale, 1990: Vagaries of Indian monsoon rainfall and its relationship with regional/global circulations, *Mausam*, **41**, pp. 301-308.
- Philander, S.G.H. and W.J. Hurlin, 1988: The heat budget of the tropical Pacific Ocean in a simulation of the 1982-83 El Niño, *Journal of Physical Oceanography*, **18**, pp. 926-931.
- Rasmusson, E. M. and T. M. Carpenter, 1983: The relationship between eastern equatorial Pacific sea surface temperatures and summer monsoon rainfall over India and Sri Lanka, *Monthly Weather Review*, **111**, pp. 517-528.
- Sasaki, Y., 1958: An objective analysis based on the variational method, *Journal of the Meteorological Society of Japan*, **36**, pp. 77-88.
- Shanno, D. F. and K. H. Phua, 1980: Remark on algorithm 500 - a variable method subroutine for unconstrained nonlinear minimization, *ACM Tran. Math. Software*, **6**, pp. 618-622.
- Shanno, D. F. and K. H. Phua, 1980: Remark on algorithm 500 - a variable method subroutine for unconstrained nonlinear minimization, *ACM Tran. Math. Software*, **6**, pp. 618-622.

- Shukla, J., 1987: Interannual variability of monsoons. In: Fein, J. S., Stephens, P. L. (Eds.) *Monsoons.*, New York: John Wiley & Sons, 632pp.
- Shukla, J., and M. Misra, 1977: Relationship between sea surface temperature and wind speed over the central Arabian Sea, and monsoon rainfall over India, *Monthly Weather Review*, **105**, pp. 998 - 1002.
- Slutz, R. J., T. J. Lubker, J. D. Hiscox, S. D. Woodruff, R. L. Jene, D. H. Joseph, P. M. Steurer, and J. D. Elms, 1985: COADS Comprehensive Ocean-Atmosphere Data Set Release 1, CIRES University of Colorado, 300 pp.
- Smith, Stuart D., 1988: Coefficients for sea surface wind stress, heat flux, and wind profiles as a function of wind speed and temperature, *Journal of Geophysical Research*, **93**, no. C12, pp. 15,467 - 15,472.
- Surgi, Naomi, 1991: Atmospheric Forcing in the Arabian Sea. USJGOFS Report No. 13.
- Verma, R.K., 1992: ENSO-Monsoon linkages as evidenced from Pacific SST correlations with monsoon precipitation. TOGA notes, no. 6.
- Weare, B. C., 1979: A statistical study of the relationship between ocean surface temperatures and the Indian monsoon, *Journal of Atmospheric Science*, **36**, pp. 2279 - 2291.
- Weare, B.C., 1989: Uncertainties in estimates of surface heat fluxes derived from marine reports over the tropical and subtropical oceans, *Tellus*, **41A**, pp. 357 - 370.
- Weare, B. C., P. Ted Strub and Michael D. Smauel, 1981: Annual mean surface heat fluxes in the Tropical Pacific Ocean, *Journal of Physical Oceanography*, **11**, pp. 705 - 717.
- Wright, Peter B., 1988: An Atlas Based on the 'COADS' Data Set: Fields of mean wind, cloudiness and humidity at the surface of the global ocean, Max-Planck-Institut für Meteorologie, Hamburg, Germany, 70pp.

Biographical Sketch

Catherine Stephens Jones was born Catherine Anne Stephens in Athens, Georgia in 1969. She grew up in Macon, Georgia. She graduated from The Florida State University in April, 1991 with a B.S. in meteorology. She is a member of the American Meteorological Society as well as Chi Epsilon Pi, the National Meteorology Honor Society. She received a NASA Global Climate Change Fellowship in 1991 for graduate work at The Florida State University. In the fall of 1992, she received her M.S. in meteorology.

Submitted papers include:

"The Effects of El Niño on Florida Rainfall and Fire Data", Catherine Stephens Jones, Jay F. Shriver, and James J. O'Brien, submitted to the *Journal of Climate*, March 1992.

"PCAs with Missing Data", James J. O'Brien and Catherine Stephens Jones, submitted to *Monthly Weather Review*, June 1992.

"The sensitivity of direct minimization techniques to parametric variations", S.D. Meyers, C. Stephens Jones, D.M. Legler, K.F. Miles and J.J. O'Brien, October 1992.